NTNU – Trondheim
Norwegian University of
Science and Technology

Electro-oxidation of ethanol at Pt electrodes with the use of a Dynamic Electrochemical Impedance Spectroscopy (DEIS) technique

Line Teigen Døssland

Chemical Engineering and Biotechnology
Submission date: June 2012
Supervisor: Frode Seland, IMTE
Co-supervisor: Per Kristian Dahlstrøm, IMT
Svein Sunde, IMT

Norwegian University of Science and Technology
Department of Materials Science and Engineering

TMT 4900 Material Chemistry and Energy Technology
Master Thesis

Electro-oxidation of ethanol at Pt electrodes with the use of a Dynamic Electrochemical Impedance Spectroscopy (DEIS) technique

Norwegian University of Science and Technology
Department of Materials Science and Engineering

Line Teigen Døssland

Supervisors:
Associate Professor Frode Seland, Per Kristian Dahlstrøm &
Svein Sunde

NTNU – Trondheim
Norwegian University of
Science and Technology

Preface

This master thesis was carried out at the Department of Materials Science and Engineering at the Norwegian University of Science and Technology.

I would like to direct appreciation to some of the people that have been involved during this project here.

I would like to thank my main supervisor Associate professor Frode Seland for guidance and support. And a special thanks to my co-supervisor Per Kristian Dahlstrøm for important guidance and help during the project both in the experimental phase and in the finishing phase. I would also like to thank my co-supervisor Svein Sunde for his involvement.

A thank you is also in place for my fellow students for good academic discussion and support during the semester.

Declaration
I declare that this work has been performed independently and in accordance with the rules and regulations at the Norwegian University of Science and Technology (NTNU).

Trondheim, June 13, 2012

Line Teigen Døssland

Abstract

Electro-oxidation of ethanol on smooth platinum surfaces was studied in the temperature range 21°C to 140°C for 0.2 M ethanol in 0.5 M sulphuric acid. This was done by use of cyclic voltammetry and electrochemical impedance spectroscopy. In addition cyclic voltammetry with different ethanol concentrations from 0.1 M to 1 M, in 0.5 M sulphuric acid was done at room temperature.

Cyclic voltammetry with different ethanol concentrations showed a shift to more positive potentials for the first oxidation peak in positive going scan as the ethanol concentration increased. A shift to more positive potentials was also observed for the oxidation peak in the negative scan as the concentration increased from 0.1 M to 1 M. This indicates that the optimum surface condition is reached at higher potentials for higher ethanol concentrations. This can be because ethanol and adsorbed ethanol derivatives take up more active sites at the surface, thus leaving less active sites available for adsorbed water derivatives which is necessary for the oxidation of ethanol to acetic acid and CO_2.

Cyclic voltammetry was done for increasing temperatures from 21°C up to 140°C for 0.2 M ethanol in 0.5 M sulphuric acid. These results showed an increase in oxidation current for all oxidation peaks as the temperature increased. A decrease in peak potential for the first oxidation peak was observed for increasing temperatures. This indicates that the optimum surface condition for ethanol oxidation is reached at lower potentials at higher temperatures. There was also seen an decrease in the apparent onset potential of the first oxidation peak as the temperature increases. These effects can come from increased thermal activity for water adsorption at higher temperatures. The peak potential for the oxidation peak in negative going scan increased with increasing temperatures. This can come from an easier reduction of platinum oxide at higher temperatures.

Dynamic electrochemical impedance spectroscopy measurements was done at different temperatures from 21°C up to 140°C for 0.2 M ethanol in 0.5 M sulphuric acid solution. The results from the measurements at 60°C was fitted to electrochemical equivalent circuits. This gave indications of one kinetically significant surface adsorbed species in most potential regions with a notable oxidation current. This in combination with literature suggesting that acetic acid and acetaldehyde is the major products from ethanol electro-oxidation suggest that the adsorbed intermediate is something other than CO(ads). Results from this work together with existing literature on ethanol oxidation was used to give a suggested simplified reaction mechanism for ethanol electro-oxidation.

Sammendrag

Elektrooksidasjon av etanol på en jevn platinaoverflate har blitt studert i temperaturområdet 21°C til 140°C for 0,2 M etanol i 0,5 M svovelsyre. Dette ble gjort ved bruk av syklisk voltammetri og elektrokjemisk impedansspektroskopi. I tillegg ble det utført syklisk voltammetri med ulike etanol konsentrasjoner fra 0,01 M til 1 M i 0,5 M svovelsyre ved romtemperatur.

Syklisk voltammetri med ulike etanolkonsentrasjoner viste en forflytning til mer positive oksidasjonspotensialer for den første oksidasjonstoppen i det positive sveipet når etanolkonsentrasjonen økte. Det ble også observert en forflytning til mer positive potensialer for oksidasjonstoppen i det negative sveipet når konsentrasjonen økte fra 0,1 M til 1 M. Dette indikerer at den optimale overflatetilstanden oppnås ved høyere potensialer for høyere etanolkonsentrasjoner. Grunnen til dette kan skyldes at etanol og andre adsorberte etanolderivater tar opp flere aktive overflatepunkter, og dermed etterlater færre ledige punkter for adsorberte vannderivater som er nødvendige for oksidasjon av etanol til eddiksyre og CO_2.

Syklisk voltammetri ble utført for økende temperaturer fra 21°C opp til 140°C for 0,2 M etanol i 0,5 M svovelsyre. Disse resultatene viste en økning i oksidasjonsstrømmen for alle oksidasjonstoppene når temperaturen økte. En nedgang i topp-potensialet ble observert for den første oksidasjonstoppen ble observert for økende temperaturer. Dette indikerer at den optimale overflatetilstanden for etanoloksidasjon oppnås for lavere potensialer ved høyere temperaturer. Det ble også sett en nedgang i det tilsynelatende startpotensialet for oksidasjonstoppen når temperaturen økte. Disse effektene kan komme av en økt termisk aktivitet for vannadsorpsjon ved høye temperaturer.

Dynamisk elektrokjemisk impedansspektroskopi ble utført ved ulike temperaturer fra 21°C opp til 140°C for 0,2 M etanol i 0,5 M svovelsyreløsning. Resultatene fra disse målingene ved 60°C ble tilpasset til elektrokjemiske ekvivalentkretser. Disse resultatene ga indikasjoner på at det er et kinetisk signifikant spesie på overflaten i potensialområdene med en merkbar oksidasjonsstrøm. Resultatene fra dEIS i kombinasjon med litteratur som foreslår at eddiksyre og acetaldehyd er hovedproduktene fra etanol elektro-oksidasjon gir grunnlag for å anta at det adsorberte mellomproduktet er noe annet en CO(ads). Resultater fra dette arbeidet ble sammen med eksisterende litteratur benyttet til å foreslå en forenklet reaksjonsmekanisme for etanol elektro-oksidasjon.

Contents

1 Introduction **1**

2 Theory **3**

2.1 Thermodynamics 3

2.2 Cyclic Voltammetry (CV) 4

2.3 Cyclic Voltammogram of Platinum in Sulphuric Acid 5

2.4 Rotating Disk Electrode (RDE) 6

2.5 Electrochemical Impedance Spectroscopy 7

2.6 Dynamic Electrochemical Impedance Spectroscopy 8

2.6.1 AC Voltammetry 8

2.6.2 FFT-dEIS 8

2.7 Electrode-Electrolyte Interphase 10

2.7.1 The Double Layer Capacity 13

2.8 Electrochemical Equivalent Circuits 13

2.8.1 Randles Ciruit 15

2.8.2 The Constant Phase Element (CPE) 16

2.9 Kinetics of Electrode Reactions 17

3 Litterature **18**

3.1 Mechanism 18

3.2 Effect of Temperature 19

4 Experimental **21**

4.1 Experimental Set Up 21

4.2 Cleaning of Glassware 21

4.3 CO-stripping 22

4.4 Cyclic Voltammetry 22

4.5 Electrochemical Impedance Spectroscopy 23
4.6 Dynamic Electrochemical Impedance Spectroscopy 24

5 Results **25**

5.1 Cyclic Voltammetry 25
5.1.1 Blank Solution, 0.5 M H_2SO_4 25
5.1.2 Carbon Monoxide (CO) 27
5.1.3 Ethanol 29
5.1.4 Ethanol Oxidation at Elevated Temperatures 33
5.2 AC Voltammograms 38
5.3 Dynamic Electrochemical Impedance Spectroscopy 40
5.3.1 Effect of temperature 47

6 Discussion **49**

6.1 DC measurements 49
6.1.1 Blank Solution, 0.5 M Sulphuric Acid 49
6.1.2 Carbon monoxide, CO 49
6.1.3 Ethanol 50
6.1.4 Effect of Temperature on Ethanol Oxidation 51
6.1.5 Different Upper Limits 52
6.2 AC measurements 53
6.2.1 AC Voltammetry 53
6.2.2 Electrochemical Impedance Spectroscopy 53
6.3 Instabilities in oxidation processes 57
6.4 Reaction Mechanism for Ethanol Oxidation 57

7 Conclusion **62**

8 Further Work **63**

A Calculation of Surface Area **a**

B Additional Dynamic Electrochemical Impedance Spectroscopy (dEIS) Measurements **b**

List of Figures

2.1 Typical triangular waveform of potential for cyclic voltammetry . . 5

2.2 Cyclic voltammogram for platinum in 0.5 M sulphuric acid, sweep rate 100 mV/s and temperature 21°C 6

2.3 Radial flow of liquid under a rotating disk electrode 7

2.4 Experimental set-up for potentiostatic EIS 8

2.5 Schematic drawing of the dEIS set-up 10

2.6 The Helmholtz double layer model is represented to the left and the Goüy-Chapman double layer model is represented to the right . . . 11

2.7 A schematic figure that shows the structure of the double layer. . . 12

2.8 A simple electrochemical surface 14

2.9 A simple equivalent circuit of an electrode interphase 14

2.10 Randles equivalent circuit 15

2.11 (a) Nyquist and (b) Bode plots for Randles circuit 16

3.1 Sketch of the mechanism for electro-oxidation of ethanol in acidic media. 18

5.1 Cyclic voltammograms for platina in 0.5 M sulphuric acid at different temperatures with a sweep rate 100 mV/s 26

5.2 Cyclic voltammograms for Pt in 0.5 M H_2SO_4 from 0.65-1.6 V with sweep rate of 100 mV/s. For temperatures from 21 to 140°C 26

5.3 Cyclic voltammograms for platinum surface in 0.5 M sulphuric acid with different reversal potentials and sweep rate of 100 mV/s 27

5.4 CO-stripping voltammogrammes at a sweep rate of 100 mV/s . . . 28

5.5 Levich plot for CO at the potential 1.05 V, whith sweep rate 100 mV/s 28

5.6 CO-stripping voltammogrammes with varying sweep rates for rotation rates of (a) 0 RPM and (b) 5000 RPM 29

5.7 Voltammogram for a Pt electrode in 0.2 M ethanol and 0.5 M H_2SO_4 at room temperature with sweep rate 100 mV/s 30

5.8 Voltammograms for 0.01, 0.1, 0.2 and 1 M ethanol in 0.5 M sulphuric acid with a sweep rate of 50 mV/s 31

5.9 Cyclic voltammograms for 200 mM ethanol at platina surface in 0.5 M sulphuric acid at 21°C with increasing sweep rates 32

5.10 Cyclic voltammetry for 0.2 M EtOH in 0.5 M sulphuric acid with 100 mV/s sweep rate at increasing temperature from 21°C up to 140°C 34

5.11 How the current changes with potential in the region 0.4-0.75 V for different temperatures with a sweep rate of 100 mV/s 35

5.12 Arrhenius plot for the potentials (a), (b), (c) and (d) for ethanol concentration 0.2 M in 0.5 M sulphuric acid with sweep rate 10 mV/s 36

5.13 Cyclic voltammograms for 200 mM ethanol at platina surface in 0.5 M sulphuric acid at 140°C with increasing sweep rates 36

5.14 Voltammograms for 0.2 M ethanol in 0.5 M sulphuric acid with different upper limits at the temperatures 21, 60, 100 and 140°C and sweep rate 100 mV/s 37

5.15 AC voltammograms at the frequencies 0.6, 5, 104 and 1040 Hz for the real and imaginary part of the admittance 39

5.16 Cyclic voltammograms acquired while performing dEIS measurements for 0.2 M ethanol in 0.5 M sulphuric acid at different temperatures with 10 mV/s sweep rate 40

5.17 Summary of EIS behaviour for 200 mM ethanol on a platinum surface in 0.5 M sulphuric acid at 60°C with 1 mV/s sweep rate . . 41

5.18 Nyquist plots acquired while doing dEIS for 700 mV at 60°C for (a) steady state and (b) 1, (c) 5 and (d) 10 mV/s sweep rate 42

5.19 Equivalent circuits used for fitting of results 43

5.20 Potential variations of charge transfer resistance, R_{ct} at 60°C 45

5.21 The potential dependence of capacitance at 60°C 45

5.22 Changes in $1/R_p$ with potential in (a) the positive scan direction and (b) negative scan direction for 60°C with 1 mV/s sweep rate . . 46

5.23 Charge transfer resistance, R_{ct} for the different temperatures is plotted versus potential in the potential region 0.5-0.7 V 47

5.24 Nyquist plots acquired while doing dEIS for 0.2 M ethanol at approximately 700 mV at different temperatures with 1 mV/s sweep rate 48

A.1 The section of a voltammogram of Pt in 0.5 M sulphuric acid at 100 mV/s used for the integration of charge for calculation of the active surface area . . . . . a

B.1 CV and EIS spectra for 0.2 M ethanol with (a) 5 mV/s and (b) 10 mV/s sweep rate at 60°C . . . . . b

List of Tables

4.1 Experimental conditions for cyclic voltammetry of ethanol containing solutions 23

4.2 Eperimental conditions for electrochemical impedance spectroscopy 24

5.1 Apparent activation energy at different potentials 35

5.2 Summary of fitting results for 60°C with 1 mV/s sweep rate 44

List of Abbreviations and Symbols

	Unit	Explanation
a	m	diameter of solvated counter ion
AC		Alternating current
AD		Analog to digital
C	$C\ V^{-1}$	Capacitance
C^*	M	Concentration of electroactive species
C_d	$C\ V^{-1}$	Differential capacitance
CPE		Constant phase element
CV		Cyclic voltammetry
D	$m^2\ s^{-1}$	Diffusion coefficient
DA		Digital to analog
DAFC		Direct Alcohol Fuel Cell
DC		Direct current
DEFC		Direct Ethanol Fuel Cell
dEIS		Dynamic Electrochemical Impedance Spectroscopy
DEMS		Differential Electrochemical Mass Spectrometry
E°	V_{SHE}	Electrode potential versus standard hydrogen electrode
E_A	$J\ mol^{-1}$	Activation energy
E_t^a	V	Positive turn-round potential
E_t^c	V	Negative turn-round potential
EIS		Electrochemical Impedance Spectroscopy
F	$C\ mol^{-1}$	Faraday constant
f	Hz	Frequency
f_{min}	Hz	Minimum frequency
FRA		Frequency Response Analyser
FFT-EIS		Fast Fourier transform electrochemical impedance spectroscopy
HNDR		Hidden negative differential resistance
k		Rate constant
j	$A\ cm^{-2}$	Current density
j_d	A	Displacement current
j_F	A	Faradaic current
R	$J\ K^{-1}mol^{-1}$	Gas constant
R_{ct}	Ω	Charge transfer resistance
R_S	Ω	Solution resistance
R_W	Ω	Warburg resistance

	Unit	Explanation
RHE		Reversible Hydrogen Electrode
Q	C	Charge
SHE		Standard Hydrogen Electrode
T	K	Temperature
Z	Ω	Impedance
α		The CPE exponent
ΔG°	kJ mol^{-1}	Standard Gibbs energy
ΔH°	kJ mol^{-1}	Standard enthalpy
$\Delta\varphi$	V	Potential difference for a parallel plate capacitor
$\varepsilon^{cell}_{C_2H_5OH/O_2}$		Energy efficiency
η	V	Overvoltage
ν	m^2 s^{-1}	Kinematic viscosity
ν_{rx}		Reaction rate
σ		Mass transfer coefficient
υ	V s^{-1}	sweep rate
ω	rad s^{-1}	Radial frequency

1 Introduction

Recent focus on human impact on the environment has led to an increasing interest of sustainable energy devices as fuel cells. Biomass derived liquid alcohol represents the ultimate fuel in a future sustainable society and can be converted to useful electrical energy in a direct alcohol fuel cell (DAFC).

Even though hydrogen represents the ideal fuel for fuel cells with water as the only by-product, low molecular weight liquid alcohols have some advantages over hydrogen when it comes to storage, transportation and handling. In addition alcohols have comparable energy densities to gasoline; ethanol has an energy density of 8.0 kWh/kg [1].

Earlier works regarding direct alcohol fuel cells have mainly been carried out on methanol. During the last years the focus have shifted from methanol to ethanol since ethanol have some advantages over methanol. Ethanol is less toxic, have a higher boiling point and can be made more easily from biomass with less energy consumption [2]. Ethanol can also be distributed through the gas station network, as is already the case in some countries like Brazil [1].

For ethanol and other carbon containing fuels the electro-oxidation occurs through a complex reaction pathway, which includes formation of intermediates at the catalyst surface. There are some drawbacks if partially oxidised products desorb from the catalyst sites. Complete oxidation of ethanol to CO_2 is desirable because it leads to the transfer of 12 electrons. The full reaction which leads to production of 12 electrons is difficult to obtain because the production of two CO_2 molecules require breaking of a C-C bond and three water molecules. Partial oxidation leads to a lower energy efficiency of the fuel cell. Another drawback is that the partially oxidized products will accumulate in the anode feed [3]. Partial oxidation of the fuel can also lead to emission of toxic by-products as acetaldehyde. The reaction mechanism for oxidation of ethanol is quite complicated and the complete oxidation requires a breaking of a C-C bond [4].

There are some known by-products from electro-oxidation of ethanol. The most commonly found and accepted by-products are acetic acid and acetaldehyde. This has been established by various IR-spectroscopy, surface enhanced Raman spectroscopy and DEMS studies [4, 5, 6].

In order to make a proper catalyst for ethanol fuel cell it is desirable to know more about the reaction kinetics of electro-oxidation of ethanol on a smooth Pt electrode surface. The aim of this project was to enhance the knowledge about the kinetics for ethanol electro-oxidation by use of electrochemical impedance spectroscopy and cyclic voltammetry. Electrochemical impedance spectroscopy

(EIS) is regarded as a method that can be used to map kinetics of an entire electrochemical system. Electrochemical impedance spectroscopy is used to map mass transport, electrochemical reactions and adsorption reactions [7].

In this project, dynamic electrochemical impedance spectroscopy (dEIS) in combination with other electrochemical techniques is used to investigate the oxidation of ethanol on a platinum surface. One advantage with dynamic electrochemical impedance spectroscopy is that it allows collection of data on the fly, which again allows study of partially covered surfaces, which is not available in conventional steady state impedance [8].

Temperature effects on ethanol electro-oxidation have been studied. This is because there is a desire to run direct ethanol fuel cells at elevated temperatures due to enhanced kinetics [1]. To look into temperature effects cyclic voltammetry and dynamic electrochemical impedance spectroscopy measurements have been done for the following temperatures from 21 to 120°C. The measurements at different temperatures were done with 0.2 M ethanol in 0.5 M sulphuric acid.

In addition to EIS measurements and cyclic voltammetry at various temperatures cyclic voltammetry were done with various ethanol concentrations (0.01, 0.1, 0.2 and 1 M) in 0.5 M sulphuric at room temperature. This was done in order to get some information about how the reaction changes with concentration.

2 Theory

2.1 Thermodynamics

In a direct ethanol fuel cell, electro-oxidation of ethanol takes place at the anode,

$$\mathrm{CH_3CH_2OH + 3H_2O \longrightarrow 2CO_2 + 12H^+ + 12e^-} \qquad \mathrm{E_1^\circ} = 0.085\ V_{\mathrm{SHE}} \tag{2.1}$$

On the cathode oxygen undergoes electro-reduction,

$$\mathrm{O_2 + 4H^+ + 4e^- \longrightarrow 2H_2O} \qquad \mathrm{E_2^\circ} = 1.229\ V_{\mathrm{SHE}} \tag{2.2}$$

$\mathrm{E_1^\circ}$ and $\mathrm{E_2^\circ}$ are the electrode potentials versus the standard hydrogen reference electrode (SHE). The total reaction corresponds to the total combustion reaction of ethanol in oxygen:

$$\mathrm{CH_3CH_2OH}(l) + 3\mathrm{O_2}(aq) \longrightarrow 2\mathrm{CO_2}(aq) + 3\mathrm{H_2O}(l) \tag{2.3}$$

The thermodynamic data for the reaction given in equation 2.3, under standard conditions, is given in equation 2.4:

$$\Delta G^\circ = -1325\ \mathrm{kJ/mol},\ \Delta H^\circ = -1366\ \mathrm{kJ/mol} \tag{2.4}$$

The given thermodynamic data give the following electromotive force at equilibrium

$$\mathrm{E_{eq}^O} = \frac{-\Delta G^O}{nF} = \frac{1325 \times 10^3}{12 \times 96,485} = \mathrm{E_2^O} - \mathrm{E_1^O} = 1.144\ \mathrm{V} \tag{2.5}$$

This gives a thermodynamic energy efficiency given by the following equation,

$$\varepsilon_{eq}^{rev} = \frac{-\Delta G^O}{-\Delta H^O} = \frac{1325 \times 10^3}{1366 \times 10^3} = 97\% \tag{2.6}$$

, where F = 96 485 C/mol is the Faraday constant, and n = 12 is the number of electrons exchanged per molecule for complete oxidation to $\mathrm{CO_2}$.

However, under working conditions the cell voltage E(j) decreases as the result of three limiting factors: The activation overpotentials, $\eta_{\mathrm{a,act}}$ and $\eta_{\mathrm{c,act}}$, the ohmic drop $\mathrm{R_e}|j|$ and the mass transfer limitations. The cell voltage can therefore be represented as

$$E(|j|) = E_2(|j|) - E_1(|j|) = \mathrm{E_2^O} + \eta_c - (\mathrm{E_2^O} + \eta_a) - R_e|j| \\ = \mathrm{E_{eq}^O} - (|\eta| + |\eta| + R_e|j|) \quad (2.7)$$

This means that the energy efficiency can be expressed as

$$\varepsilon^{cell}_{\mathrm{C_2H_5OH/O_2}} = \frac{n_{exp}FE(j)}{-\Delta H^O} = \frac{n_{exp}}{n}\frac{E(j)}{\mathrm{E_{eq}^O}}\frac{nF\mathrm{E_{eq}^O}}{-\Delta H^O} \\ = \frac{n_{exp}}{n}\frac{E(j)}{\mathrm{E_{eq}^O}}\frac{\Delta G^O}{\Delta H^O} = \varepsilon_F\varepsilon_E\varepsilon^{rev}_{eq} \quad (2.8)$$

Thus, for a DEFC working at 0.5 V at 50 mA/cm^2 and leading either to CO_2 (complete oxidation), acetic acid (partial oxidation) or acetaldehyde (partial oxidation) the overall efficiency would be

$$\varepsilon^{cell}_{\mathrm{C_2H_5OH/O_2}} = \frac{12}{12} \times \frac{0.5}{1.144} \times 0.97 \approx 42.4\% \quad (2.9)$$

$$\varepsilon^{cell}_{\mathrm{C_2H_5OH/O_2}} = \frac{4}{12} \times \frac{0.5}{1.144} \times 0.97 \approx 14\% \quad (2.10)$$

$$\varepsilon^{cell}_{\mathrm{C_2H_5OH/O_2}} = \frac{2}{12} \times \frac{0.5}{1.144} \times 0.97 \approx 7\% \quad (2.11)$$

respectively. Because ε^{rev}_{eq} is determined by thermodynamics, this expression shows that the only ways to increase the overall efficiency significantly are to increase ε_F and to increase ε_E. ε_F can be increased by favouring the complete oxidation to CO_2 and ε_E can be increased by decreasing the overvoltages, η and the ohmic drop, $R_e|j|$ [9].

2.2 Cyclic Voltammetry (CV)

Cyclic voltammetry involves the process of imposing a potential with a triangular waveform on the working electrode while simultaneously measuring the current. The triangular waveform of the potential is shown in Figure 2.1, where E_t^a and E_t^c are the positive and negative turn-round potentials, respectively. In aqueous electrolytes E_t^c and E_t^a are chosen to lie between the hydrogen and oxygen evolution potentials, from about 50 mV and up to 1.6 V, depending on the sweep rate

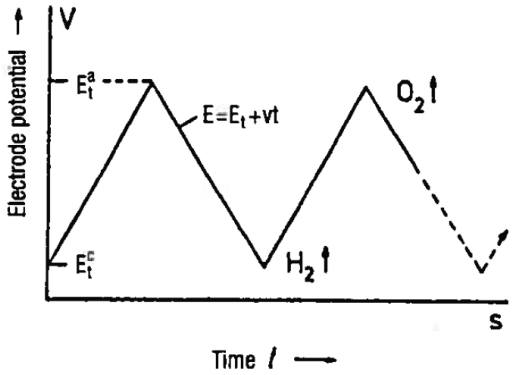

Figure 2.1: Typical triangular waveform of potential for cyclic voltammetry [10]

and temperature. The sweep rate, v, is the change of potential with time [10]. Charging of the double layer will occur when there is a change in potential and give a small current response. The current response of surface processes is proportional to sweep rate while mass transport controlled processes have a current response that is proportional to the square root of the sweep rate. The coupling of charge and mass transfer will therefore determine the current. For fast charge transfer processes there is a peak potential that is independent of sweep rate. For slow charge transfer processes the peak potential position will shift with varying sweep rate [10].

2.3 Cyclic Voltammogram of Platinum in Sulphuric Acid

Figure 2.2 shows the cyclic voltammogram for platinum in 0.5 M sulphuric acid in room temperature with sweep rate 100 mV/s. The lower and upper potential limit was 0.05 V and 1.6 V respectively. In potentials lower than 0.35 V when sweeping downwards there will be adsorption of hydrogen at the platinum surface. For potentials lower than 0.35 V when sweeping upwards there will be desorption of hydrogen from the platinum surface. Adsorption and desorption of hydrogen are reversible processes, this can be seen from the butterfly peaks for adsorption and desorption. The region between 0.35 and 0.8 V is the double layer region, where the current only comes from charging of the double layer. For potentials higher than approximately 0.75 V platinum starts to oxidise and form an oxide layer with different catalytic properties. The reduction of the oxide happens at a more negative potential, which is an indication that platinum oxidation is an irreversible reaction.

The hydrogen adsorption peak can be used to calculate the real active surface

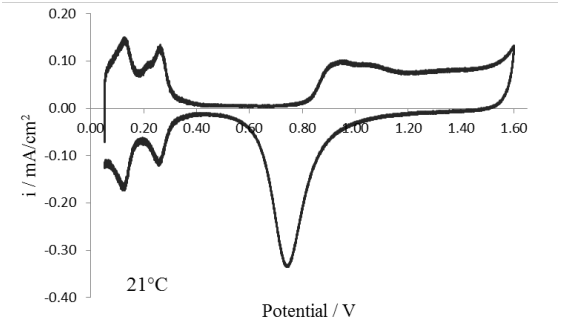

Figure 2.2: Cyclic voltammogram for platinum in 0.5 M sulphuric acid, sweep rate 100 mV/s and temperature 21°C

area of the electrode. This can be done by assuming that there is one hydrogen per surface platinum atom and a surface charge equal to 220 μCcm^{-2} [11]. See Appendix A to see how this was done.

2.4 Rotating Disk Electrode (RDE)

There are three common modes for mass transfer in solutions; diffusion, migration and convection. One experimental method which involves forced convection is the rotating disk electrode. The working electrode for this method is a disk of the electrode material that is embedded in a non-conducting material. The rod is rotated by a motor and rotated at a certain frequency, f, where the parameter of interest is the angular frequency $\omega = 2\pi f$ [12].

The radial flow of liquid under a rotating disk electrode is shown in Figure 2.3. The flow on the electrode surface is laminar, but there is one small layer on the electrode surface that is left unstirred where the mass-transfer is diffusion controlled. This layer is called the Nernst diffusion layer [10].

For a totally mass-transfer-limited condition at the RDE the following equation also known as the Levich equation is valid [12]

$$j_{l,c} = 0.620nFAD^{2/3}\omega^{1/2}\nu^{-1/6}C^* \tag{2.12}$$

, where $j_{l,c}$ is the limiting current density, n is the number of electrons transferred, F is the Faraday constant, D is the diffusion coefficient, ν is the kinematic viscosity and C^* the concentration of electroactive species.

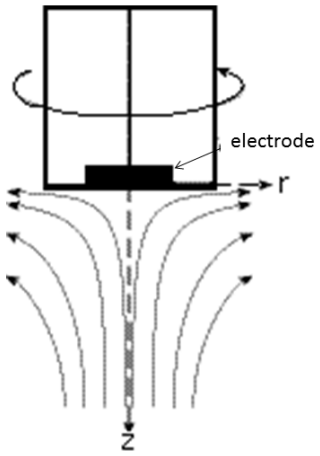

Figure 2.3: Radial flow of liquid under a rotating disk electrode

2.5 Electrochemical Impedance Spectroscopy

Electrochemical impedance spectroscopy (EIS) is an electrochemical method which allows us to gain information about the electrical double layer, the reaction interface and the reactions taking place at the interface. In potentiostatic EIS the system is exposed to a small a.c. sine wave on top of the d.c. potential [13]. The angular frequency, ω is varied and the measured result is the impedance, Z.

Figure 2.4 shows the experimental setup for potentiostatic EIS. The figure shows that there is a function generator that generates a sine wave with small amplitude. This is applied to the electrochemical cell together with a d.c. voltage through a potentiostat. The current now contains both an a.c. and a d.c. part. The a.c. parts (amplitude and phase) from both current and potential are separated and analysed by a Frequency Response Analyser (FRA). The amplitude and the phase of the current and potential are converted into a value of the impedance at the frequency of the sine wave. These measurements are repeated for different frequencies, which makes it possible to build up an impedance spectrum.

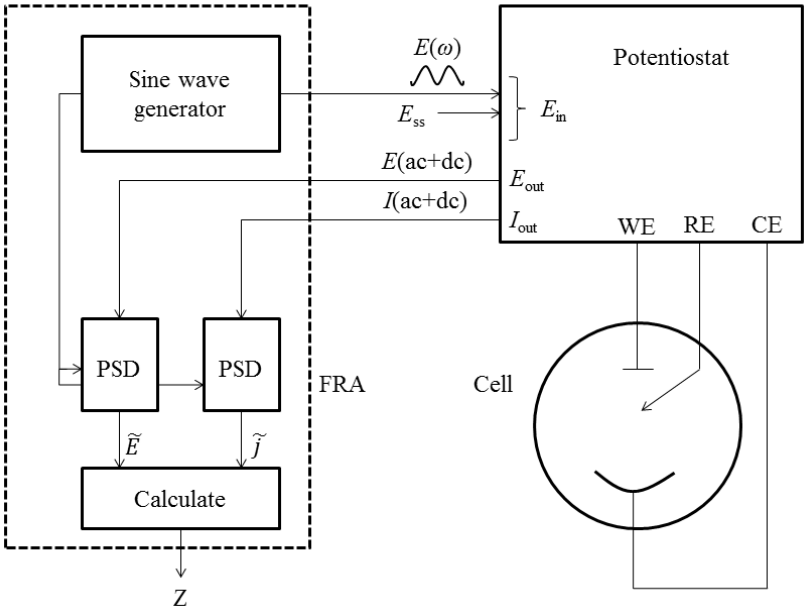

Figure 2.4: Experimental set-up for potentiostatic EIS, modified figure from Harrington [14]

2.6 Dynamic Electrochemical Impedance Spectroscopy

2.6.1 AC Voltammetry

AC voltammetry is a variation of the standard potentiostatic EIS, in this method there is a slowly changing "d.c." potential. On top of this it is applied a small a.c. sine wave. The experiments are repeated with the same slowly changing "d.c." potential with a.c. sine waves of different frequencies. Extracting and calculating the impedance for each frequency and potential, EIS spectra around the voltammogram can be presented, as done by Harrington (1993) [15].

2.6.2 FFT-dEIS

Dynamic electrochemical impedance spectroscopy (dEIS) with fast Fourier transfer analysis is a modified version of a.c. voltammetry. FFT-dEIS allows multiple sine waves to be added and simultaneously applied to the working electrode. Such a potential waveform is continuously applied on top of a slowly varying "d.c" potential. This method can be used to continuously acquire impedance spectra around a cyclic voltammogram.

Fast Fourier Transform methods have been used in the field of electrochemical impedance spectroscopy (EIS) for a while and have recently been used in the study of non-stationary processes. This has been made possible by improvements of instrumentation during generations of computer technology [8]. However, dynamic electrochemical impedance spectroscopy (dEIS) based on FFT-EIS have some experimental constraints.

One experimental constrain for electrochemical impedance spectroscopy is that the amplitude of the a.c. voltage must be small enough to be considered a perturbation of the d.c. voltage [12]. Roy et al. (2004) found that a condition for a.c. voltammetry which is also applicable for FFT-EIS is that the rate of variations in the d.c. voltage must be smaller than the rate of variations of the a.c. voltage [16]. They also found that the variation in current density should not be large. Sacci and Harrington [8] have found that for their work these restrictions were satisfied if they maintained the following relationship between sweep rate, υ, and minimum frequency, $f_{\min}$

$$f_{\min} = 200V^{-1} \cdot \upsilon \tag{2.13}$$

This relationship is also assumed valid throughout this work.

The setup used for dEIS measurements in this work is quite similar to the one described by Sacci and Harrington [8]. The setup is shown schematically in Figure 2.5. It consists of a digital to analog (DA) converter and three analog to digital converters (AD). The Digital to analog converter (DA0) is used to output the potential ramp and multisine waveform into a potentiostat. The large known E_{dc} component is subtracted off from the total potential measured by the potentiostat and leaves the AC component. The AC component is then amplified to near full scale by the AD converter AD1. The DC component of the potential is then recorded by the AD converter AD2. The DC and AC current are recorded together by AD0.

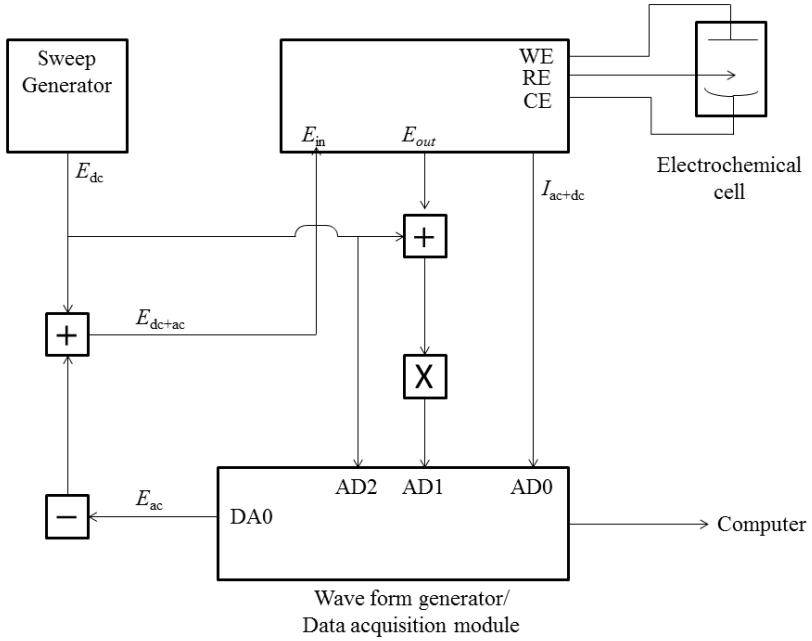

Figure 2.5: A schematic drawing of the dEIS setup described by Sacci and Harrington [8]

2.7 Electrode-Electrolyte Interphase

Because of its high dielectric constant water is a good solvent for ions. This leads to charging of most metal surfaces in water. Surface charges lead to formation of an electric field which attracts counter ions. This layer of surface charges and counter ions is called the electrical double layer [17].

When an electrical double layer is formed at an electrode it is possible to find an excess of ions with charge opposite to the charge on the electrode on the solution side of the phase boundary. A simple way to imagine the double layer is to imagine that these ions approach the surface of the electrode as close as possible, as shown to the left in Figure 2.6. Here it is possible to see that the double layer consists of two parallel layers of charge. This model was suggested by Helmholtz and is now named the Helmholtz-layer model. The separation of the layers is a/2, where a is the diameter of the solvated counter ion [10, p. 116].

The Helmholtz model of the electrical double layer is incomplete and does not sufficiently describe the double layer. This is because it does not take account for thermal motion of ions and fails to explain the capacitance of the electrical double layer. The model has therefore been developed further by Goüy and Chapman in

1910-1917. This led to the development of a theory with a diffuse double layer that is more extended than the Helmholtz layer [17, 10]. The Goüy-Chapman model with the diffuse double layer is shown to the right in Figure 2.6.

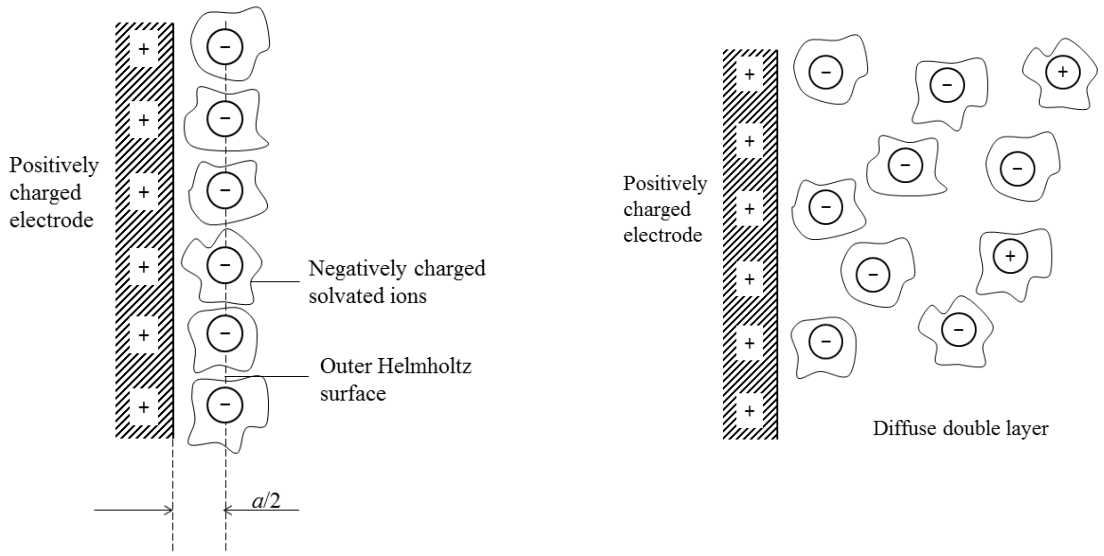

Figure 2.6: The Helmholtz double layer model is represented to the left and the Goüy-Chapman double layer model is represented to the right

It was later pointed out by Stern that a more realistic model is a combination of the diffuse double layer and the Helmholtz layer. Another important point is that the position of the Helmholtz plane will vary with the size and type of ion attracted to the surface. This lead to development of a model with an inner Helmholtz plane consisting of ions which have lost their solvation and is attached very closely to the surface and an outer Helmholtz plane with ions that is solvated. A figure that shows this model is shown in Figure 2.7. [17, 10]

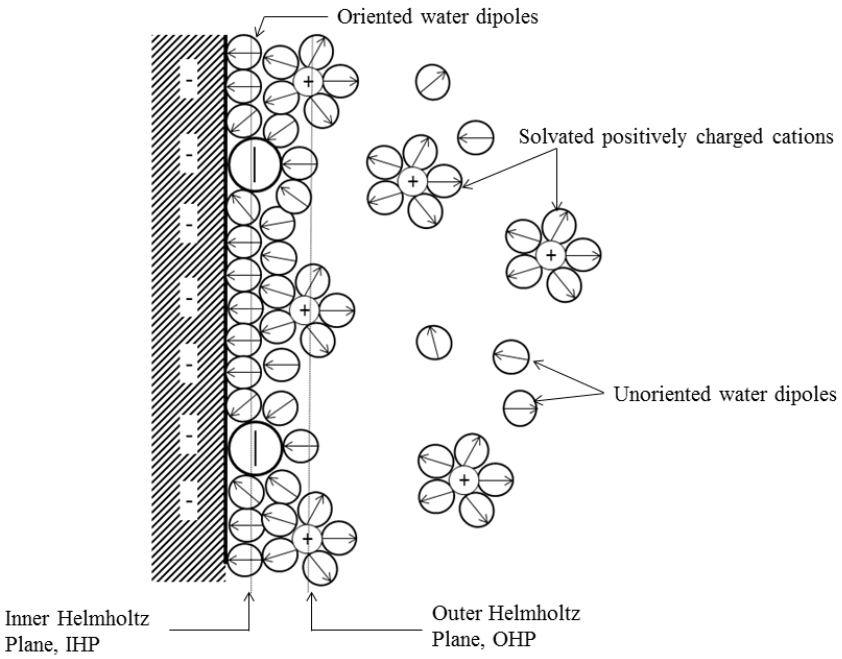

Figure 2.7: A schematic figure that shows the structure of the double layer.

2.7.1 The Double Layer Capacity

The simplest way to consider the electrical double layer is to compare it to a parallel plate capacitor. There is a linear relationship between the charge, Q, and the potential difference between the plates, $\Delta\varphi$ for such capacitors. The proportionality constant is the capacitance, C, as given in Equation 2.14 [10].

$$Q = C\Delta\varphi \tag{2.14}$$

For the electrical double layer, Q is the excess charge on the solution side of the interface. and $\Delta\varphi$ is the potential difference between the metal and solution. It is most correct to compare the electrical double layer to a parallel plate capacitor when the double layer is best described by the Helmholtz model.

There is one important difference between the capacitance of the electrical double layer and the capacitance of a parallel plate capacitor. The capacitance of a parallel plate capacitor is independent of potential while the capacitance of the electrical double layer is dependent of the potential and is therefore better described by dq/dE than the value of C itself. This value is often referred to as the differential capacitance C_d as given i Equation 2.15 [10].

$$C_d = dQ/dE \tag{2.15}$$

2.8 Electrochemical Equivalent Circuits

A simple electrochemical system can be imaged as two parallel plates where the reaction happens at the electrode and the potential is measured against a reference electrode. A simple sketch showing a surface in an electrochemical system with currents from the surface is shown in Figure 2.8. A generalized example of an electrochemical reaction is given in Equation 2.16.

$$\mathrm{O} + n\mathrm{e}^- \rightleftharpoons \mathrm{R} \tag{2.16}$$

In Figure 2.8 j_F is the Faradaic current and j_d is the displacement current. The Faradaic current, j_F, comes from the electrochemical reactions and the displacement current, j_d, comes from charging of the double layer. This model leads to a simple equivalent circuit with a capacitance in parallel with a resistor and a resistor in series with this system. The Equivalent circuit for this simple electrochemical system is shown in Figure 2.9.

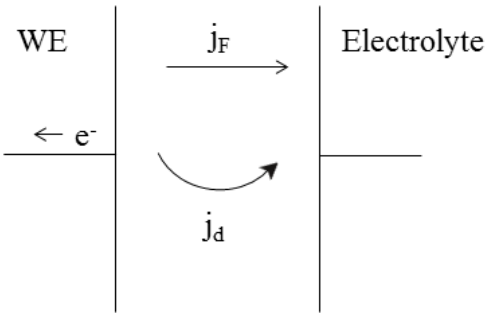

Figure 2.8: A simple electrochemical surface, where WE is the working electrode, j_F is the Faraday current and j_d is the displacement current.

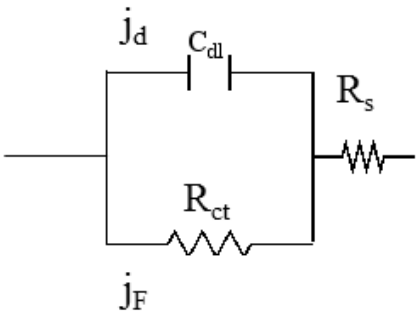

Figure 2.9: A simple equivalent circuit of an electrode interphase. j_F is the Faradaic current, j_d is the displacement current, R_{ct} is the resistance for charge transfer and R_S is the solution resistance.

In Figure 2.9 R_{ct} is the resistance for charge transfer and R_s is the solution resistance. C_{dl} is the double layer capacitance. The current j is the sum of j_d and j_F as written in Equation 2.17.

$$j = j_d + j_F \tag{2.17}$$

The impedance of an ideal resistor is real as shown in Equation 2.18

$$Z_R = R \tag{2.18}$$

While the impedance of an ideal capacitor is purely imaginary as shown in Equation 2.19.

$$Z = \frac{1}{i\omega C} \tag{2.19}$$

2.8.1 Randles Ciruit

A one step reaction with semi-infinite diffusion can be described by Randles Circuit shown in Figure 2.10.

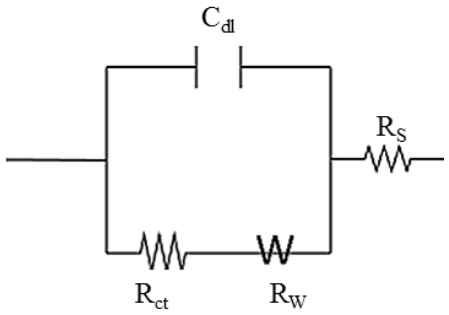

Figure 2.10: Randles equivalent circuit

In this figure R_s is the resistance of the solution, R_{ct} is the charge transfer resistance, C_{dl} is the double layer capacitance and R_W is the Warburg resistance. The Warburg element, W, is an equivalent circuit element for diffusion and the impedance of the Warburg element is given by Equation 2.20.

$$Z_W = \frac{\sqrt{2}}{\sqrt{i}} \frac{\sigma}{\sqrt{\omega}} \tag{2.20}$$

In Equation 2.20 i is the imaginary unit, $\omega = 2\pi f$ is the angular frequency and σ is the mass transfer coefficient as given in Equation 2.21 for an electrochemical reaction as the one given in Equation 2.16.

$$\sigma = \sigma_O + \sigma_R = \frac{RT}{n^2 F^2 \sqrt{2}} \left[\frac{1}{\sqrt{D_O} C_O(0)} + \frac{1}{\sqrt{D_R} C_R(0)} \right] \tag{2.21}$$

In Equation 2.21 σ_O and σ_R is the mass transfer contributions of specie O and R respectively. D_O and D_R is the diffusion coefficient of specie O and R respectively and $C_O(0)$ and $C_R(0)$ is the surface concentrations of specie O and R.

The Nyquist plot and the Bode plot for Randles circuit is given in Figure 2.11

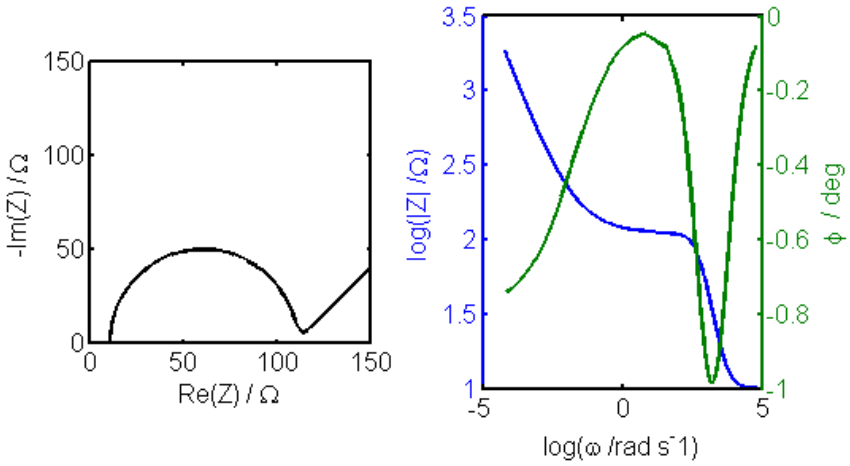

Figure 2.11: (a) Nyquist and (b) Bode plots for Randles circuit, with $R_s = 10$, $R_ct = 100$, $\sigma = 10$, and $C = 20 \cdot 10^{-6}$

2.8.2 The Constant Phase Element (CPE)

The impedance response of electrodes is rarely ideal. There will often be time-constant dispersions due to variations along the surface. Presence of time-constant (or frequency) distributions is often modelled by use of a constant phase element (CPE) [7]. A CPE's impedance is given by Equation 2.22.

$$\mathrm{Z}_{CPE}(\omega) = \frac{1}{Q(i\omega)^{\alpha}} \tag{2.22}$$

Where Q is a proportionality factor with numerical value and α is the CPE exponent which characterizes the phase shift. When $\alpha = 1$, 0, -1 CPE represents an ideal capacitor, C, an ideal resistor, R, or an ideal inductor, L, respectively [18]. One accepted explanation for the CPE is surface roughness, which causes coupling of solution resistance and double layer capacitance. But this does not always explain the CPE behaviour another reason for the CPE behaviour may be uneven distribution of the double layer capacitance across the surface. It is also a possibility that the CPE is an intrinsic property of the double layer [19].

2.9 Kinetics of Electrode Reactions

Rate constants for solution-phase reactions are known to vary with temperature in a common fashion. Arrhenius was the first to recognise that ln$k$ is linear with $1/T$ and he proposed that the rate constant could be expressed in the following form

$$k = Ae^{-E_A/RT} \tag{2.23}$$

Where k is the rate constant, A is a constant often called the frequency factor, E_A is the activation energy and R is the gas constant [12].

The current of an electrochemical reaction is given by Equation 2.24.

$$j = nF\nu_{rx} \tag{2.24}$$

Where n is the number of electrons transferred, F is the Faraday constant and ν_{rx} is the reaction rate.

The reaction rate depends on the rate expression, concentration of reactants and k, because of this the reaction rate, ν_{rx} is proportional to k with each other.

This means that ln$j$ is proportional with ln$k$ and that an Arrhenius plot with ln$j$ against 1/T should give a straight line. This can be used to estimate the apparent activation energy, E_A. The apparent activation energy can then be estimated from the results of the regression and from Equation 2.25

$$\ln j = A' + \left(-\frac{E_A}{R}\right)\frac{1}{T} \tag{2.25}$$

Where j is the current, A' is a constant, E_A is the apparent activation energy, R is the gas constant and T is the temperature.

3 Litterature

3.1 Mechanism

The mechanism for electro-oxidation of ethanol on platinum catalysts is still not fully understood, but there have been done some experimental and theoretical studies to get an increased understanding of the mechanism. The mechanism for oxidation of ethanol goes through adsorbed intermediates at the surface. A simplified mechanism for electro-oxidation of ethanol in acidic media, was suggested by Krewer et al., and is reproduced in Figure 3.1 [3].

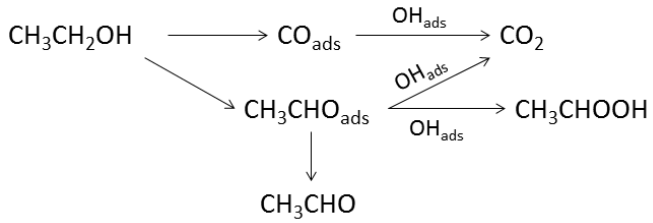

Figure 3.1: Sketch of the mechanism for electro-oxidation of ethanol in acidic media.

Vigier et al. (2004) did studies of the mechanism by use of electrochemical methods and in situ IR reflectance spectroscopy. From these studies and existing literature they concluded that the adsorbed intermediates were CO and CH_3CO. Furthermore, they showed that CH_3CHO acted both as intermediate and final product. They also determined that CH_3COOH, CO_2 and CH_4 were final products [4]. This corresponds to what Hitmi et al. (1994) found in their kinetic study of electro-oxidation of ethanol. They found that the number of electrons transferred in the region up to 0.8 V was 2 to 2.5 which corresponds mainly to the oxidation of ethanol to acetaldehyde and that for the region of 0.8 V to approximately 1.5 V the mean number of electrons transferred was 3.5 to 4 which corresponds mainly to the electro-oxidation of ethanol to acetic acid [20].

Lai et al. (2008) did a study on the mechanism of ethanol and acetaldehyde electro-oxidation by use of surface enhanced Raman spectroscopy (SERS) where they observed C_1 species at potentials as low as 0.10 V. This suggests that C-C bond breaking can occur at low potentials. They also observed an additional carbon fragment which was identified as CH, which can be further oxidized to CO and CO_2. The quantity of adsorbed species was higher for acetaldehyde than for ethanol. This suggests that C-C scission occurs more readily for acetaldehyde than ethanol and that acetaldehyde is a likely intermediate for oxidation of ethanol to CO_2 [5].

Wang, Jusys and Behm (2004) did a study of ethanol electro-oxidation in acidic media on a platina catalyst. They studied the reaction by a combination of electrochemical methods and differential electrochemical mass spectrometry (DEMS). They looked into effects of concentration and temperature. Results from this study indicates that acetaldehyde and acetic acid is the main products when doing cyclic voltammetry with sweep rate 10 mV/s, 0.01 M ethanol in 0.5 M sulphuric acid at 60°C. The average yield of acetic acid and acetaldehyde was 35% and 45% respectively, while the average yield of CO_2 was 5.1%. Another conclusion from this study was that for DEFC with carbon supported Pt-catalysts it will be necessary to operate ethanol fuel cells at higher temperatures to avoid emission of toxic by-products (acetaldehyde) and to accomplish complete oxidation to CO_2 [6].

Brateng (2005) have studied methanol and ethanol oxidation by use of cyclic voltammetry, potential step methods, rotating disk electrode and electrochemical quarts crystal nanobalance [21]. She observed differences in the massograms for ethanol and methanol for potentials below 0.65 V vs RHE, suggesting that the strongly adsorbed species are different.

Camara and Iwasita (2005) have done an in-situ FTIR-spectroscopy study of ethanol electro-oxidation at 0.5 V for different ethanol concentrations in perchloric acid [22]. Their experimental work suggests that there is a maximum for CO_2 production at 0.025 M ethanol and a decrease in CO_2 production for higher concentrations. They did not detect acetaldehyde at concentrations lower than 0.1 M ethanol, but for higher concentrations acetaldehyde seemed to be the predominant product.

3.2 Effect of Temperature

There have been done some studies that have looked into the effect of temperature on ethanol oxidation. Colmati, Antolini and Gonzalez (2006) did a study on the effect of temperature on carbon supported Pt, PtRu and Pt_3Sn catalysts. Their focus was mainly on comparing the different catalysts performance at different temperatures. They concluded that the Pt/C had an overall poor performance at all temperatures and that the Pt_3Sn/C catalyst showed the best high temperature performance [23].

Sun et al. (2009) did a high temperature/high pressure differential electrochemical mass spectroscopy (DEMS) study of ethanol electro-oxidation on carbon supported catalysts. In this study they found that the current efficiency of carbon dioxide formation depends on concentration of ethanol, reaction temperature, electrolyte flow rate and electrode potential. Their results suggest that the CO_2 current

efficiency increases with decreasing concentrations of ethanol and that it increases with increasing temperatures. They also found that the CO_2 current efficiency is depending on the electrode potential. Their results indicated that the current efficiency for CO_2 evolution was almost negligible at low temperatures, the maximum at 60°C was 5%. In their work they did not have the possibility to separate between the production of acetic acid and acetaldehyde because the thin non porous teflon membrane between the mass spectrometer chamber and the electrochemical thin-layer flow cell inhibited permeation of larger molecules as acetic acid and acetaldehyde. This allowed them to only separate between complete and incomplete oxidation and not between the products [24].

Only sparse studies on ethanol oxidation by impedance spectroscopy have been done. Pierozynski (2012) have looked into kinetics of ethanol electro-oxidation by cyclic voltammetry and a.c. voltammetry [25]. The results from this work showed that electro-oxidation of ethanol shows a great temperature dependence. This could be seen from an Arrhenius plot for the peak current in the positive sweep direction and a reduction in the charge transfer resistance with temperature for ethanol electro-oxidation for 0.25 M ethanol. Although kinetic information was retrieved from impedance data, no attempt was done to correlate these with a plausible reaction mechanism. However, a simple R(QR) circuit was used to fit the data in most potential regions allowing only a very simple mechanism to be used.

4 Experimental

The following sections will give a description of the experimental procedure used during this project including cleaning of glassware and electrodes and the electrochemical experiments. All potentials were measured against a reversible hydrogen electrode (RHE).

4.1 Experimental Set Up

The experimental set up for CO-stripping was consisting of a one-compartment glass cell which contained a working electrode, which was rotating disk electrode (RDE) of polycrystalline platina from Pine instruments, a counter electrode of platina and a reversible hydrogen electrode as reference.

The experimental set up used for cyclic voltammetry of ethanol, electrochemical impedance spectroscopy and dynamic electrochemical impedance spectroscopy during this project included a glass autoclave (miniclave from Büchi Glas Uster AG) which contained a working electrode of platina, a counter electrode also made of platina and a reversible hydrogen electrode in the same solution as the reference electrode (internal reference) as the reference electrode. The internal reference was preferred over an external one due to easy handling, even though the reference potential might be susceptible for changes with temperature.

4.2 Cleaning of Glassware

The glassware and electrodes used during this project was first rinsed in distilled water (Millipore Milli-Q 18.2 MΩ), cleaned in hot concentrated sulphuric acid (95% AnalaR normapur VWR Prolabo) and then rinsed in distilled water again. Some parts of the autoclave was made out of polytetrafluorethylene, these were rinsed in distilled water and cleaned in a hot peroxide bath until there was no bubbles left on the surface. Peroxide bath for cleaning consisted of 150 mL distilled water (Millipore Milli-Q 18.2 MΩ), and approximately 60 mL hydrogen peroxide (30wt% Sigma Aldrich). After cleaning in the peroxide bath the parts were rinsed in distilled water again.

4.3 CO-stripping

The potentiostat used for CO-stripping was a Gamry Reference 600^{TM}, utilizing Gamry Instruments Electrochemistry Software. There was done an activation and cleaning of the working electrode prior to CO-stripping. This was done by doing cyclic voltammetry in 0.5 M sulphuric acid solution with 100 mV/s sweep rate while purging the solution with Argon gas (Yara Praxair AS) to avoid effects from oxygen. After activation it was done cyclic voltammetry of 0.5 M sulphuric acid at different sweep rates while the solution still was purged with Argon gas. The cyclic voltammograms of the blank solution was processed in Echem analyst and used for determination of the surface area of the working electrode.

After cyclic voltammetry of blank solution carbon monoxide gas (Linde 4.7) was bubbled into the 0.5 M sulphuric acid solution while doing cyclic voltammetry at a sweep rate of 100 mV/s until the cyclic voltammogram obtained was stable. The bubbling of CO gas continued throughout the experiments to ensure saturated solution. Cyclic voltammetry was performed at different sweep rates and different rotation speeds. The sweep rates used were in the range 10 mV/s to 1000 mV/s. And the rotation rates was in the range 0 RPM to 5000 RPM.

4.4 Cyclic Voltammetry

Cyclic voltammetry was carried out with different concentrations of ethanol (99.9% ethanol for spectroscopy, Merck) in room temperature and for 0.2 M ethanol at different temperatures (from 21°C to 140°C). The supporting electrolyte was 0.5 M sulphuric acid, which was prepared from 96% H_2SO_4 Merck, Suprapur and Millipore Milli-Q 18.2 MΩ distilled water.

Cyclic voltammetry in 0.5 M sulphuric acid was carried out at 100 mV/s until the cyclic voltammogram seemed unchanged to activate and clean the working electrode. Argon gas (Yara) was purged into the solution while doing this to clean the solution from oxygen. After the activation was finished the autoclave was closed tightly and heated to the appropriate temperature. Prior to cyclic voltammetry of ethanol it was also carried out cyclic voltammetry of blank solution at the different temperatures with different sweep rates. At room temperature it was also carried out cyclic voltammetry with the following reversal potentials; 0.7, 0.9, 1.1, 1.3 and 1.6 V. The potentiostat used for carrying out the cyclic voltammetry was a Gamry Reference 600^{TM}, utilizing Gamry Instruments Electrochemistry Software. The cyclic voltammograms of the blank solution was processed in Echem analyst as described in Appendix A and used for determination of the surface area of the working electrode.

The ethanol was added directly into the autoclave in proper amounts through an opening in the lid. The autoclave was cooled down before addition of the ethanol. After the ethanol was added the solution was purged with argon gas again to remove possible amounts of oxygen and to mix the solutions.

A summary of the different experimental conditions for cyclic voltammetry of solutions containing ethanol is given in Table 4.1.

Table 4.1: Experimental conditions for cyclic voltammetry of ethanol containing solutions

Ethanol Conc. M	Sweep Rates mV/s	Upper Limit V	Temperature °C
0.01	10, 20, 50, 100, 200, 500	1.6	21
0.01	100	1.2, 1.4, 1.6	21
0.1	10, 20, 50, 100, 200, 500	1.6	21
0.1	100	1.2, 1.35, 1.6	21
0.2	10, 20, 50, 100, 200, 500, 1000	1.6	21
0.2	100	0.7, 0.9, 1.1, 1.3, 1.6	21
1	10, 20, 50, 100, 200, 500	1.6	21
1	100	0.6, 0.95, 1.1, 1.3, 1.6	21
0.2	10, 20, 50, 100, 200, 500, 1000	1.6	40
0.2	100	0.7, 0.9, 1.1, 1.3, 1.6	40
0.2	10, 20, 50, 100, 200, 500, 1000	1.6	60
0.2	100	0.7, 0.9, 1.1, 1.3, 1.6	60
0.2	10, 20, 50, 100, 200, 500, 1000	1.6	80
0.2	100	0.7, 0.9, 1.1, 1.3, 1.6	80
0.2	10, 20, 50, 100, 200, 500, 1000	1.6	100
0.2	100	0.7, 0.9, 1.1, 1.3, 1.6	100
0.2	10, 20, 50, 100, 200, 500, 1000	1.6	120
0.2	100	0.7, 0.9, 1.1, 1.3, 1.6	120
0.2	10, 20, 50, 100, 200, 500, 1000	1.6	140
0.2	100	0.7, 0.9, 1.1, 1.3, 1.6	140

4.5 Electrochemical Impedance Spectroscopy

Electrochemical Impedance Spectroscopy was carried out for 0.2 M ethanol at different temperatures. The solutions and the temperatures were the same as for cyclic voltammetry. The experiments were done by holding the potential steady for a while prior to doing impedance measurements at some different potentials. The potentiostat used for doing the electrochemical impedance measurements was

a Gamry Reference 600^{TM}. The summary of concentrations, temperature and potentials for electrochemical impedance spectroscopy is given in Table 4.2.

Table 4.2: Eperimental conditions for electrochemical impedance spectroscopy

Ethanol Conc. M	Potential V	Temperature °C
0.2	0.55, 0.60, 0.65, 0.75, 0.80, 0.85, 0.90, 0.95, 1.25, 1.30, 1.35	21
0.2	0.55, 0.60, 0.65, 0.75, 0.80, 0.85, 0.90, 0.95, 1.25, 1.30, 1.35	40
0.2	0.55, 0.60, 0.65, 0.75, 0.80, 0.85, 0.90, 0.95, 1.25, 1.30, 1.35	60
0.2	0.55, 0.60, 0.65, 0.75, 0.80, 0.85, 0.90, 0.95, 1.25, 1.30, 1.35	80
0.2	0.55, 0.60, 0.65, 0.75, 0.80, 0.85, 0.90, 0.95, 1.25, 1.30, 1.35	100
0.2	0.55, 0.60, 0.65, 0.75, 0.80, 0.85, 0.90, 0.95, 1.25, 1.30, 1.35	120
0.2	0.55, 0.60, 0.65, 0.75, 0.80, 0.85, 0.90, 0.95, 1.25, 1.30, 1.35	140

4.6 Dynamic Electrochemical Impedance Spectroscopy

Dynamic electrochemical impedance spectroscopy was done for 0.2 M ethanol at different temperatures. The temperatures and solutions used were the same as for cyclic voltammetry and electrochemical impedance spectroscopy. The experimental setup and theory for dynamic electrochemical impedance spectroscopy is explained in 2.6.2. The sweep rates used were 1 mV/s, 5 mV/s and 10 mV/s. The minimum frequency was set to 0.2 Hz for 1 mV/s sweep rate and 2 Hz for sweep rates of 5 and 10 mV/s. EIS spectra were fitted to equivalent circuits using ZSimpWin. The F-ratio test [26, 27] was used to confirm when it was necessary to add extra elements to the circuits. The F-ratio test with a and $2N$-n degrees of freedom for adding a parameters to give n parameters in the new circuit is

$$F = \frac{(\chi^2(n-1) - \chi^2(n))/a}{\chi^2(n)/(2N-n)} \tag{4.1}$$

Where N is the number of frequencies. The acceptance limit chosen was that the chance that F was going to be exceeded was less than 1%.

5 Results

5.1 Cyclic Voltammetry

Some results from the cyclic voltammetry experiments done during this work is given in the following section. All the potentials performed on a smooth Pt electrode and measured against a reversible hydrogen electrode (RHE).

5.1.1 Blank Solution, 0.5 M H_2SO_4

This section gives a presentation of the results from cyclic voltammetry of blank solution. Figure 5.1 shows how the cyclic voltammograms for blank solution changes with the temperature for a sweep rate of 100 mV/s. In this figure it is possible to observe the typical hydrogen adsorption and desorption peaks at the lowest potential. At the highest potentials platinum oxide is formed at the surface. The platinum oxide is reduced during the negative sweep. In the region between the hydrogen and oxide region is the double layer region.

Figure 5.1 shows that that the peak current density for hydrogen adsorption and desorption changes little with increasing temperature. It also shows that the peak current density for oxygen production and reduction of platinum oxide increases with temperature at a given sweep rate. However, increased amount of oxide is generated at the highest temperatures, which can be seen by the following increased reduction peak on the negative-going scan.

Figure 5.2 shows how the cyclic voltammogram for blank solution changes with temperature in the higher potential region when the sweep rate is 100 mV/s. This figure shows that the onset potential for platinum oxide production decreases with increasing temperatures and that the slope in the onset of the oxide region gets steeper with increasing temperatures. The onset potential for the oxide region decreases from 0.82 V to 0.77 V as the temperature is increased from 21°C to 140°C. The figure also shows that the peak potential for oxide reduction is increasing with increasing temperatures, from 0.73 V at room temperature to 0.77 V at 140°C.

Figure 5.3 shows cyclic voltammograms with varying upper reversal potentials in blank solution (0.5 M sulphuric acid) at 21°C and 100 mV/s. From this figure it is possible to see that the potential for the onset of the platinum oxide reduction peak is increasing as the upper limit for the cyclic voltammetry is reduced. The peak potential for the reduction shifted to more positive potentials when the reversal potential of the cyclic voltammetry is reduced.

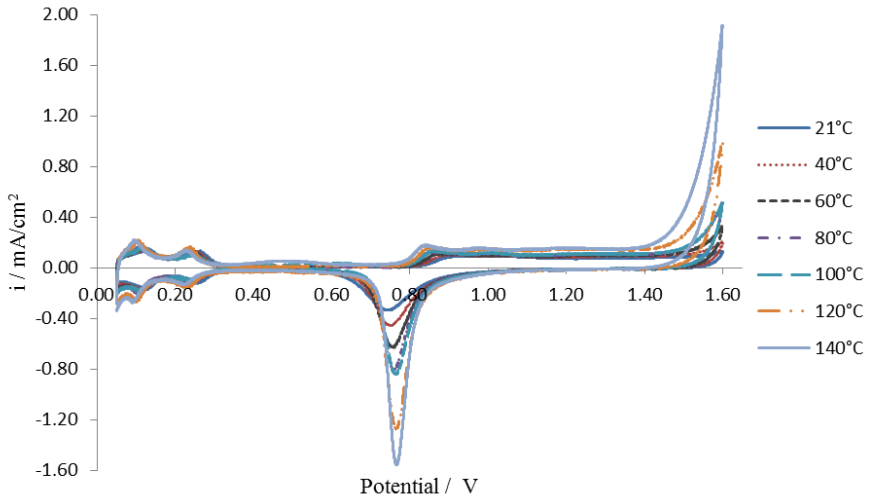

Figure 5.1: Cyclic voltammograms for platina in 0.5 M sulphuric acid at different temperatures with a sweep rate 100 mV/s

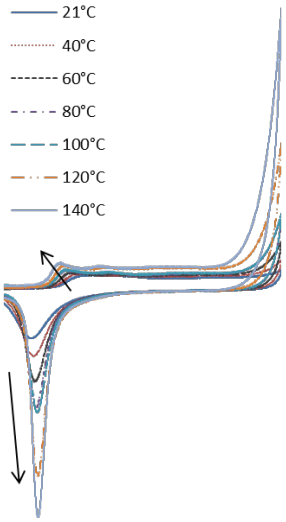

Figure 5.2: Cyclic voltammograms for Pt in 0.5 M H_2SO_4 from 0.65-1.6 V with sweep rate of 100 mV/s. For temperatures from 21 to 140°C

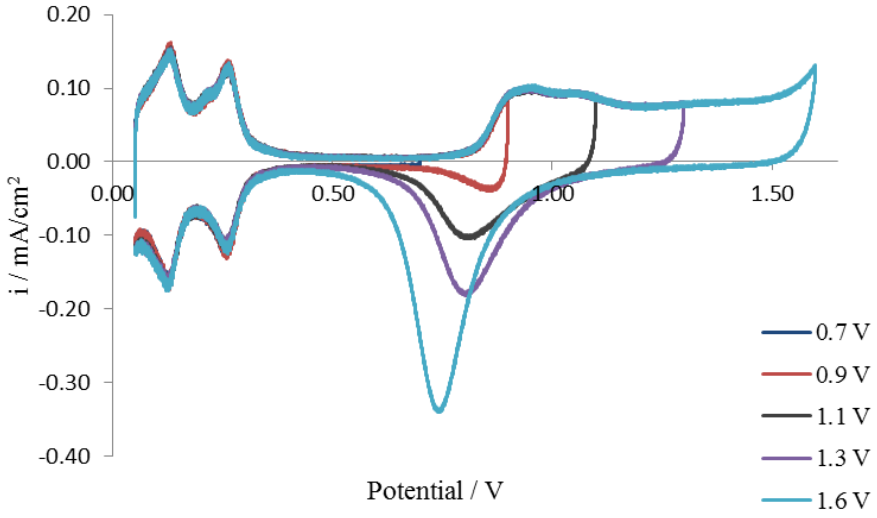

Figure 5.3: Cyclic voltammograms for platinum surface in 0.5 M sulphuric acid with different reversal potentials and sweep rate of 100 mV/s

5.1.2 Carbon Monoxide (CO)

Cyclic voltammetry of a carbon monoxide (CO) saturated solution of sulphuric acid was performed at room temperature, approximately 21°C. Figure 5.4 (b) shows how the cyclic voltammogram for CO-stripping changes with varying rotation rates when the sweep rate was 100 mV/s. Figure 5.4 (a) is given for comparison and shows how the current is cahnging with potential for rotation rate of 0 RPM and 100 mV/s sweep rate.

At potentials below 0.9 V no current is observed, thus the surface seems to be completely blocked by adsorbed CO. The sharp peak that can be observed at approximately 0.9 V for all the rotation rates corresponds to fast oxidation of the CO adsorption layer. After this there is a reduction in the current density. The current density in the region after the peak at approximately 0.96 V is increasing with rotation rate.

The Levich plot for CO oxidation at 1.05 V, right after the oxidation peak, is given in in Figure 5.5. This is a plot of the current density versus the square root of the rotation frequency, $\omega^{1/2}$ in rad/s. This figure shows an approximately straight line for the change of current density with the square root of the rotational frequency.

Figure 5.6 shows how the current density changes with potential for a CO saturated solution of 0.5 M sulphuric acid solution at a platinum RDE when the rotation rate is 0 RPM and 5000 RPM. The current density in the region

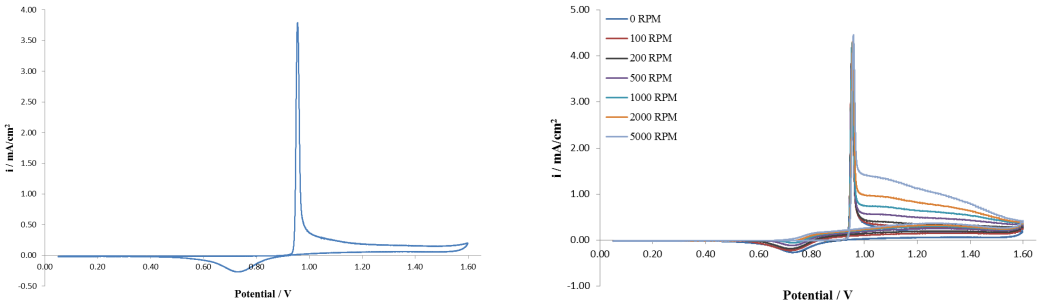

(a) (b)

Figure 5.4: CO-stripping voltammogrammes for (a) 0 RPM and (b) varying rotation rates at a sweep rate of 100 mV/s

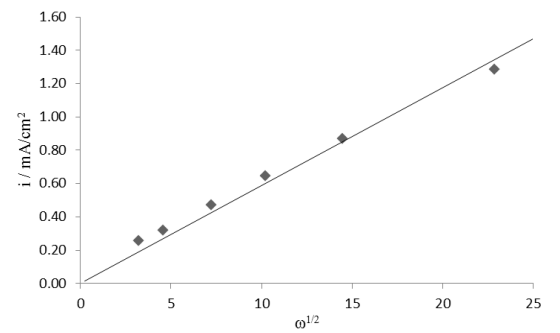

Figure 5.5: Levich plot for CO at the potential 1.05 V, whith sweep rate 100 mV/s

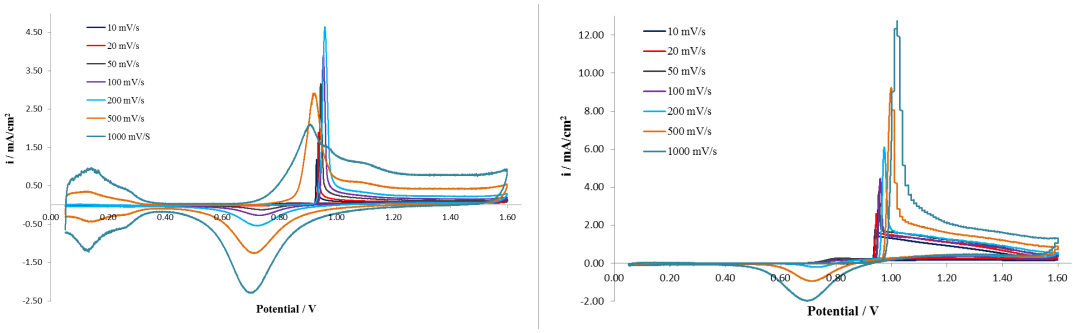

(a) (b)

Figure 5.6: CO-stripping voltammogrammes with varying sweep rates for rotation rates of (a) 0 RPM and (b) 5000 RPM

between 0.9 V and 1.6 V is lower for 0 RPM than for 5000 RPM. Furthermore, Figure 5.6 shows a less pronounced stripping peak for high sweep rates for 0 RPM than for lower sweep rates. This is because CO(aq) is not given enough time to adsorb completely at the very high sweep rates, destabilizing the adsorbed layer and allowing it to be oxidized at more negative potentials [28].

5.1.3 Ethanol

Cyclic voltammetry was performed for different concentrations of ethanol in 0.5 M sulphuric acid solution at room temperature (21°C). A typical cyclic voltammogram for 0.2 M ethanol in 0.5 M sulphuric acid at room temperature, 21°C, with a sweep rate of 100 mV/s is given in figure 5.7 together with a voltammogram for platinum in 0.5 M sulphuric acid alone for comparison. Ethanol oxidation at Pt yields two oxidation peaks in positive scan and one oxidation peak in the negative scan. Where the first oxidation peak in positive going scan has a peak potential and a peak current density of 0.95 V and 70 mA/cm^2 respectively. The second oxidation peak in the positive going scan has a peak potential of 1.35 V and a peak current of 0.97 mA/cm^2. The oxidation peak in the negative going scan has a peak potential of 0.65 V and a peak current density of 1.5 mA/cm^2 A reduction peak is also observed in the negative-going scan corresponding to the Pt reduction peak, with a peak potential of 0.81 and a peak current density of -0.14 mA/cm^2.

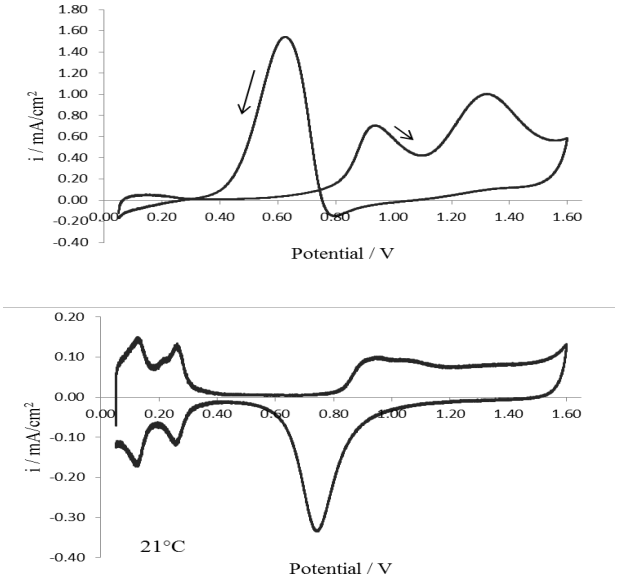

Figure 5.7: Voltammogram for a Pt electrode in (a) 0.2 M ethanol and 0.5 M sulphuric acid at room temperature(21°C) and (b) 0.5 M sulphuric acid. The sweep rate is 100 mV/s

The voltammograms for 0.01, 0.1 and 1 M ethanol in 0.5 M sulphuric acid with a sweep rate of 50 mV/s is shown in Figure 5.8, together with a voltammogram for 0.5 M sulphuric acid for comparison.

Figure 5.8 shows that the cyclic voltammograms of ethanol in sulphuric acid have some changes with increasing concentration. The first oxidation peak in the positive going scan have the following peak potentials and peak currents increases as the concentration increases from 0.85 V and 0.12 mA/cm^2 for 0.01 M to 0.95 V and 1.9 mA/cm^2. This gives an clear indication that the peak potentials and peak currents for the first oxidation peak increases with increasing ethanol concentration. The peak potentials for the second oxidation peak in the positive scan direction is 1.35 V, 1.35 V and 1.27 V for 0.01 M, 0.1 M and 1 M ethanol respectively. While the peak currents for the same concentrations in the same order is; 0.11, 0.52 and 1.27 mA/cm^2 respectively. From this it is clear that an increase in concentration gives an increase in peak current for the second peak in positive going scan.

The figure shows a clear increase in peak current with increasing concentration for the oxidation peak in negative going scan. The peak currents for this peak is 0.18 mA/cm^2 for 0.01 M, 0.92 mA/cm^2 for 0.1 M, and 2.5 mA/cm^2 for 1 M. The peak potentials for the oxidation peak in negative going scan is 0.61 V for 0.01 M,

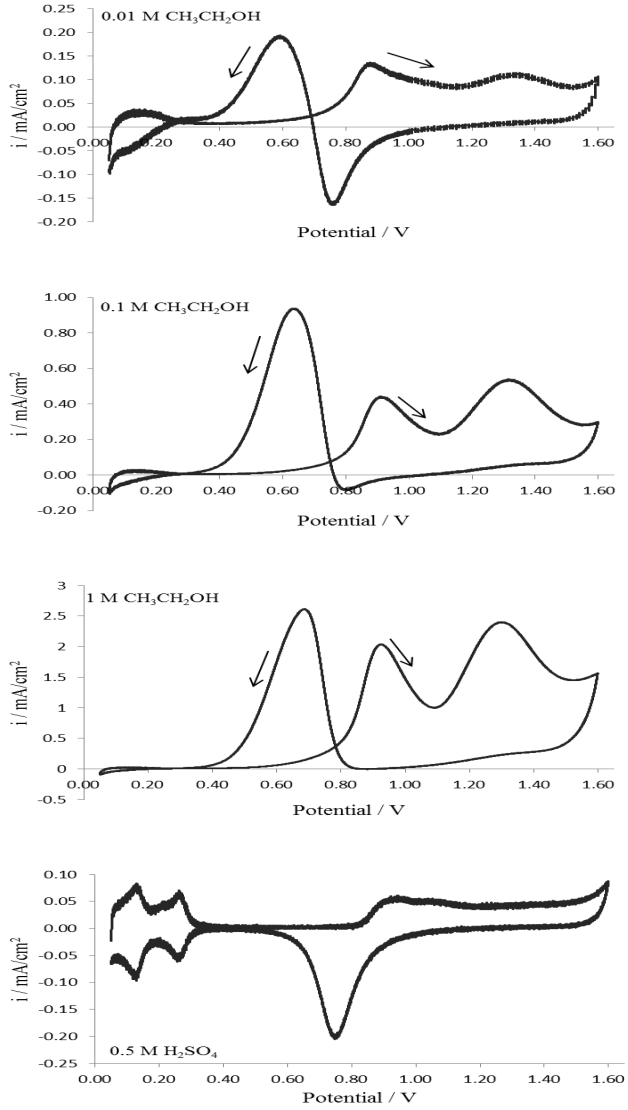

Figure 5.8: Voltammograms for 0.01, 0.1, 0.2 and 1 M ethanol in 0.5 M sulphuric acid with a sweep rate of 50 mV/s

0.65 V for 0.1 M, and 0.70 V for 1 M. This clearly shows that the potential for the oxidation peak in negative going scan increases for increasing concentrations of ethanol.

The reduction peak in the negative going scan leading to the oxidation peak occurring at 0.78 for 0.1 M ethanol is getting less and less visible when the ethanol concentration increases. At the same time, the following oxidation peak increases

in size and the peak shifts to more positive potentials until eventually, at 1 M ethanol concentration, the reduction is not visible anymore. This reduction peak corresponds to reduction of the platinum oxide layer formed during the positive-going scan, which is essentially constant, independent of ethanol concentration.

Figure 5.9 shows how the cyclic voltammograms for 200 mM ethanol in sulphuric acid changes with increasing sweep rates in room temperature (21°C). The current density for the first oxidation peak in the positive scan direction increases with increasing sweep rate when the sweep rate is over 100 mV/s. At lower sweep rates the peak current seems to be unchanged, but the peak potential shifts a little towards more negative potentials as the sweep rate is lowered. However, the starting point for the peak seems to be unchanged (around 0.55 V) with sweep rate. For the second peak it is easier to observe a clear trend. The peak current increases and shifts towards more positive potentials with increasing sweep rates.

A clear trend also seems to be observable for the reduction peak in the negative going scan. This peak has increasing absolute value for the current density with increasing sweep rates. The figure also shows that the position of anodic peak shifts to more negative potentials with higher sweep rates. The oxidation peak in negative scan direction has increasing peak current density with increasing sweep rates. This peak also seems to shift to lower potentials with increasing sweep rates.

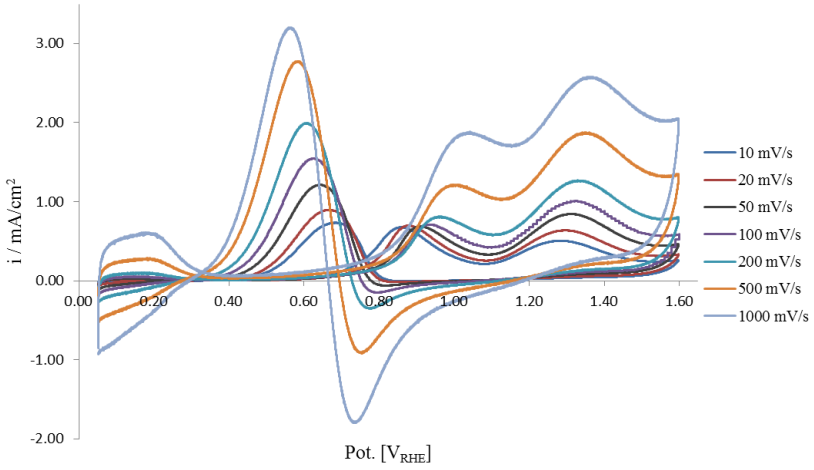

Figure 5.9: Cyclic voltammograms for 200 mM ethanol at platina surface in 0.5 M sulphuric acid at 21°C with increasing sweep rates

5.1.4 Ethanol Oxidation at Elevated Temperatures

Cyclic voltammetry was done for 0.2 M ethanol at increasing temperatures. Figure 5.10 shows the voltammogram for 0.2 M ethanol in 0.5 M sulphuric acid with 100 mV/s sweep rate for increasing temperatures from 21°C up to 140°C. The peak current density for the first peak in the positive going scan increases from 0.70 mA/cm^2 at room temperature to 38 mA/cm^2 at 140°C. While the peak potential showed a small decrease with temperature from about 0.95 V at room temperature to 0.88 V at 140°C. The second oxidation peak in the positive going scan has a peak potential of 1.35 at 21°C, 1.25 V at 60°C and 1.18 at 140°C, which indicates that the peak potential for the second peak decreases with temperature. The peak current density for the second peak increased from 0.98 to 8.9 mA/cm^2 when going from room temperature to 140°C. The peak current for the oxidation peak in negative scan direction increases from 1.5 mA/cm^2 at room temperature to 99 mA/cm^2 at 140°C. The peak potential for the same peak increased with temperature from 0.64 V at room temperature to 0.79 V at 140°C.

Clearly, the first oxidation peak is lower than the second oxidation peak at room temperature. As the temperature increases this changes and the first oxidation peak in positive scan direction becomes larger than the first peak. The anodic peak in the reverse scan direction is not visible at the higher temperatures. Furthermore, the oxidation peak in the reverse scan gets larger and sharper, than at lower temperatures.

From Figure 5.10 it seems like the first oxidation peak in the positive direction starts at a lower potential at higher temperatures than at lower temperatures. Another interesting feature seen in Figure 5.10 is that there is a shoulder on the negative side of the first oxidation peak at elevated temperatures, which shifts towards even more negative potentials at higher temperatures. At 60°C this shoulder is visible at potentials around 0.65 V and at 140°C it is visible at 0.58 V.

Figure 5.11 shows how the current changes with potential in the potential region 0.4-0.75 V for forward scan with sweep rate 100 mV/s at different temperatures. This figure further emphasise that the potential starts increasing at lower potentials when the temperature increases. The apparent onset potential is around 0.55 V at room temperature and around 0.45 V at 140°C Even though it looks like there is a change in the onset potential it is possible to observe a current all the way down to the H_{UPD} area for all temperatures.

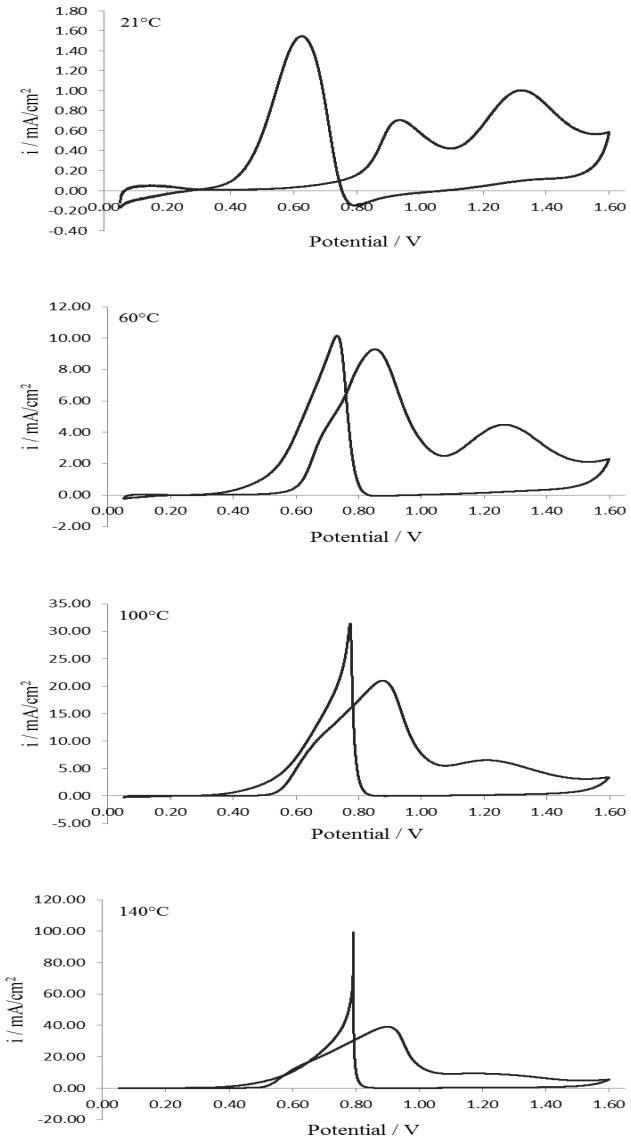

Figure 5.10: Cyclic voltammetry for 0.2 M EtOH in 0.5 M sulphuric acid with 100 mV/s sweep rate at increasing temperature from 21°C up to 140°C

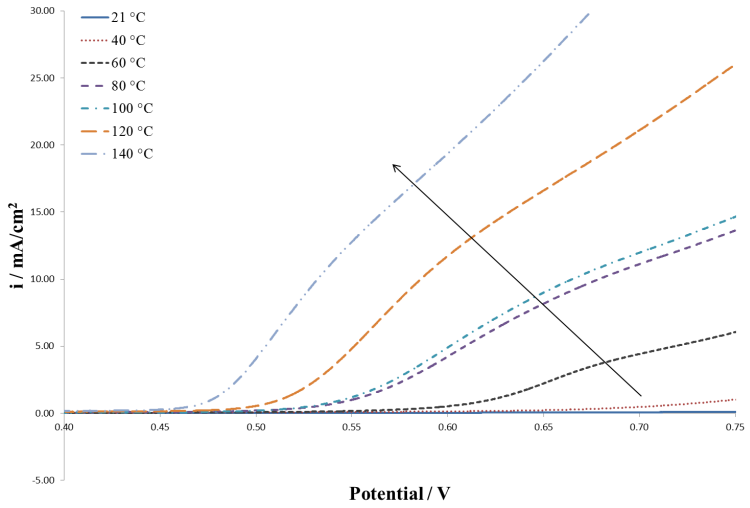

Figure 5.11: How the current changes with potential in the region 0.4-0.75 V for different temperatures with a sweep rate of 100 mV/s

Table 5.1: Apparent activation energy at different potentials

Potential V	Apparent Activation Energy, E_A kJ/mol
0.5	54.8
0.6	47.0
0.7	40.6
0.8	35.8

Plots of the logarithm of current versus 1/T were made for the following potentials; 0.5, 0.6, 0.7 and 0.8 V. These plots are given in Figure 5.12. The slopes calculated by linear regression from this figure were used to estimate the apparent activation energy at the four different potentials by the following equation

$$\ln j = A' + \left(-\frac{E_A}{R}\right)\frac{1}{T} \tag{5.1}$$

Where j is the current, A' is a constant, E_A is the apparent activation energy, R is the gas constant and T is the temperature.

The estimated activation energies is given in Table 5.1.

From Table 5.1 it is possible to see that the apparent activation energy, E_A decreases as the potential increases.

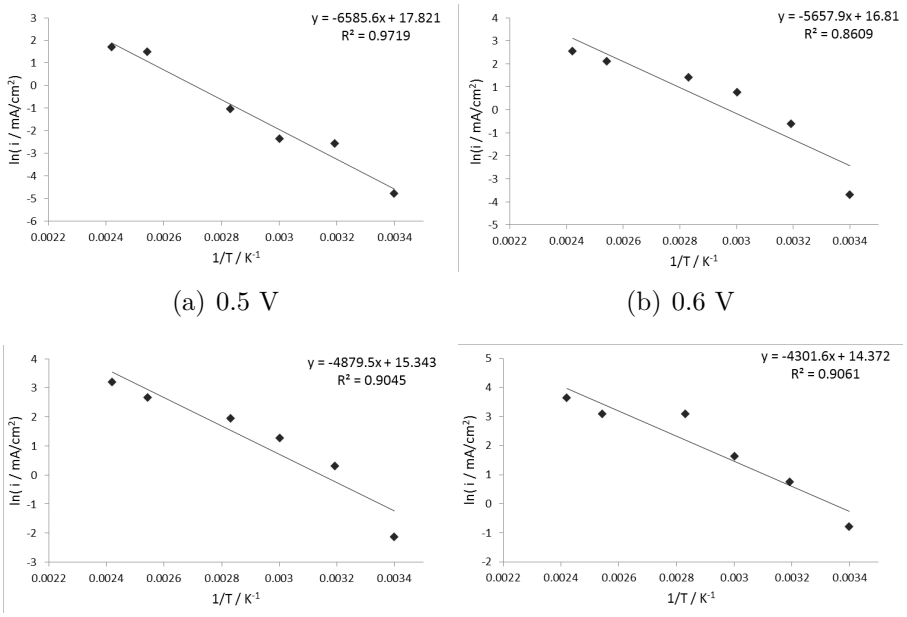

(a) 0.5 V (b) 0.6 V

(c) 0.7 V (d) 0.8 V

Figure 5.12: Arrhenius plot for the potentials (a), (b), (c) and (d) for ethanol concentration 0.2 M in 0.5 M sulphuric acid with sweep rate 10 mV/s

Figure 5.13 shows how the cyclic voltammograms for 200 mM ethanol in sulphuric acid changes with increasing sweep rates at 140°C.

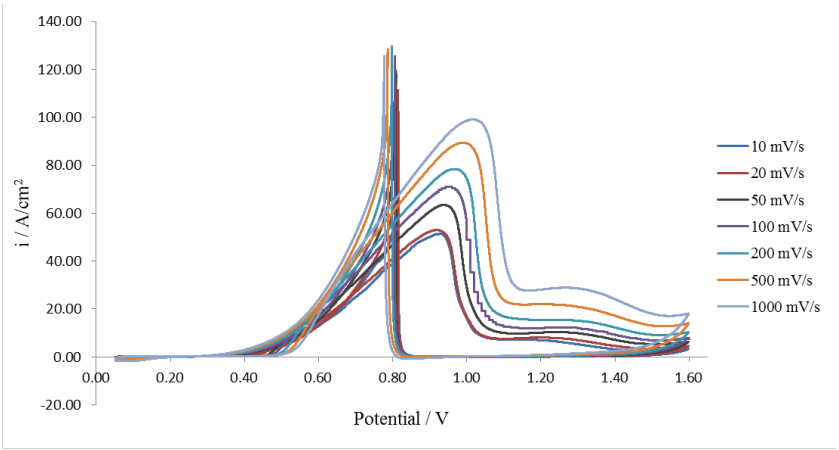

Figure 5.13: Cyclic voltammograms for 200 mM ethanol at platina surface in 0.5 M sulphuric acid at 140°C with increasing sweep rates

From Figure 5.13 it is possible to see that some of the same trends observed for increasing sweep rates in room temperature, given in Figure 5.9, are visible at

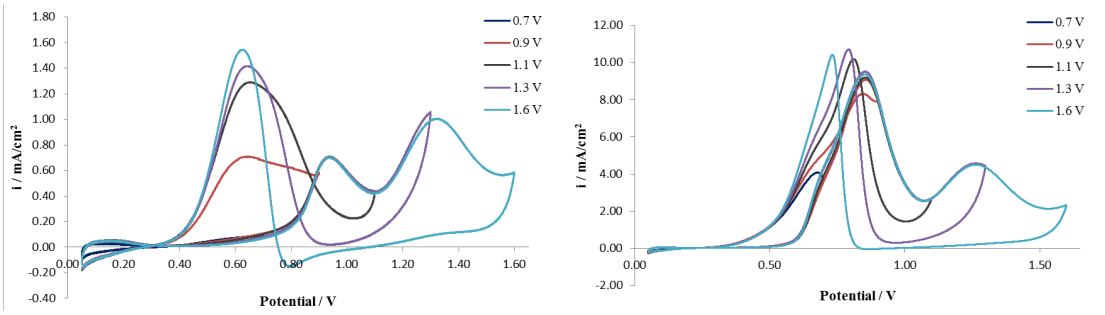

(a) 21°C

(b) 60°C

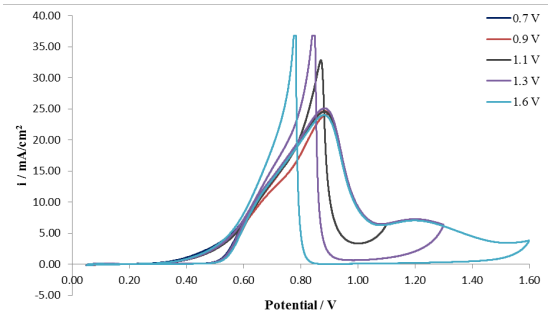

(c) 100°C

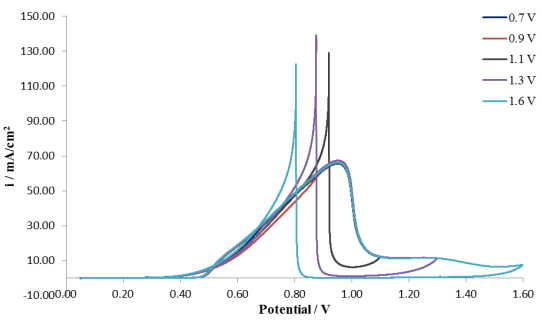

(d) 140°C

Figure 5.14: Voltammograms for 0.2 M ethanol in 0.5 M sulphuric acid with different upper limits at the temperatures 21, 60, 100 and 140°C and sweep rate 100 mV/s

140°C. Although there are some distinct differences. The current density for the first peak is increasing with increasing sweep rates from 10 mV/s up to 1000 mV/s, and shifts to more positive potentials. The peak potential is 0.90 V with sweep rate 10 mV/s and 1.01 V for sweep rate 1000 mV/s.

Experiments were done with different upper limits for the cyclic voltammetry with ethanol concentration of 0.2 M at different temperatures. Some of the results from these experiments is shown in Figure 5.14.

Figure 5.14 shows how the voltammograms for ethanol in sulphuric acid changes with different upper limits for some temperatures. From this figure it seems that there is little changes in either peak current density or peak potential for the peak at approximately 0.9 V in the forward scan direction at room temperature. It is possible to observe more changes for the oxidation peak at approximately 0.6 V in the negative going scan at room temperature. The peak current decreases with decreasing upper limits, from 1.6 mA when the reversal potential was 1.6 V and to 1.3 mA/cm^2 when the reverse potential was 1.1 V. The peak potential seem to increase with decreasing upper limit, when the reverse potential was 1.6 V the

peak potential was 0.64 V and for reverse potential of 1.1 V there was a peak potential of 0.68 V.

There are some similarities between the voltammograms with varying upper limits in room temperature and for higher temperatures. It is not possible to see a trend for how the oxidation peak current density for the oxidation peak for reverse scan changes with increasing reversal potentials at higher temperatures. The peak potential for the oxidation peak in negative going scan seems to decrease with increasing reversal potentials at all temperatures. From 0.85 when the reversal potential was 1.1 V to 0.78 V for a reversal potential of 1.6 V at 100°C. The peak potential and peak current for the first peak in the forward scan direction changes little with changing upper limits for all the temperatures. And can be seen at 0.7 V, 24 mA/cm^2 for 100°C and at 0.95 V, 66 mA/cm^2 for 140°C.

5.2 AC Voltammograms

Examples of AC voltammograms that represent the raw data for the impedance spectra for dEIS measurements at 60°C with sweep rate of 1 mV/s is given in Figure 5.15.

An observation that can be made from Figure 5.15 is where the real or imaginary admittance goes through zero. This information can tell us something about how the Nyquist diagram will look like. When the real part of the admittance becomes negative it is usual to observe that the the spectra are moving into the second or third quadrant. A negative imaginary admittance will indicate that the spectra is moving into the third or fourth quadrant [29].

The AC voltammograms shown in Figure 5.15 shows that both the real and negative part of the admittance show negative values at lower frequencies. From this figure it is also possible to see that it is an increase in the value of the imaginary part of the admittance around 800 mV in positive scan direction for the higher frequencies, and that there is a reduction in the imaginary admittance for higher frequencies around the same potential. This figure gives a good indication about how the capacitance changes with potentials, because the imaginary part of the admittance for higher frequencies mostly represent the double layer capacitance.

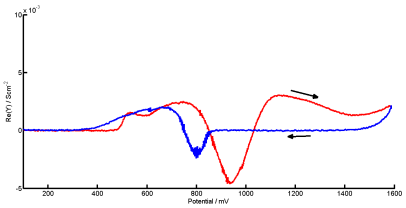

(a) 0.6 Hz

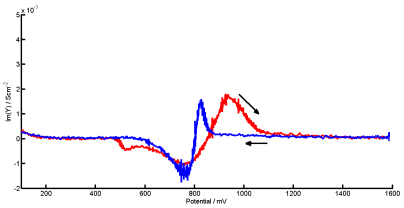

(b) 0.6 Hz

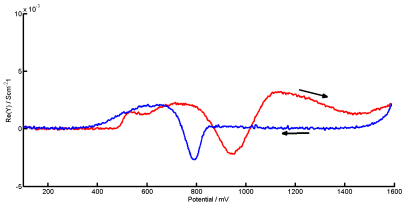

(c) 5 Hz

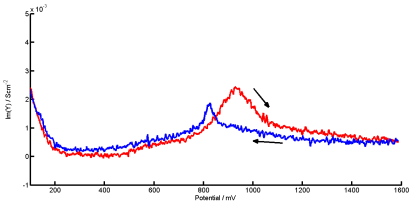

(d) 5 Hz

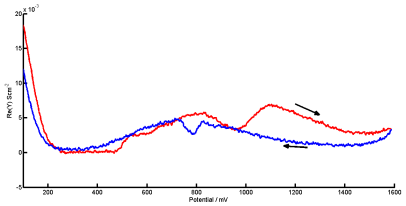

(e) 104 Hz

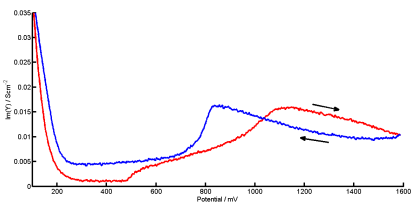

(f) 104 Hz

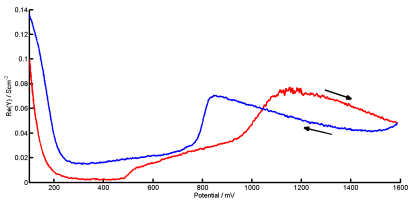

(g) 1040 Hz

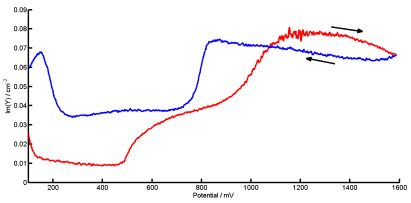

(h) 1040 Hz

Figure 5.15: AC voltammograms at the frequencies 0.6, 5, 104 and 1040 Hz for the real and imaginary part of the admittance

5.3 Dynamic Electrochemical Impedance Spectroscopy

An approximate representation of the cyclic voltammograms recorded while doing the dynamic electrochemical impedance spectroscopy at different temperatures with a sweep rate of 10 mV/s is given in Figure 5.16.

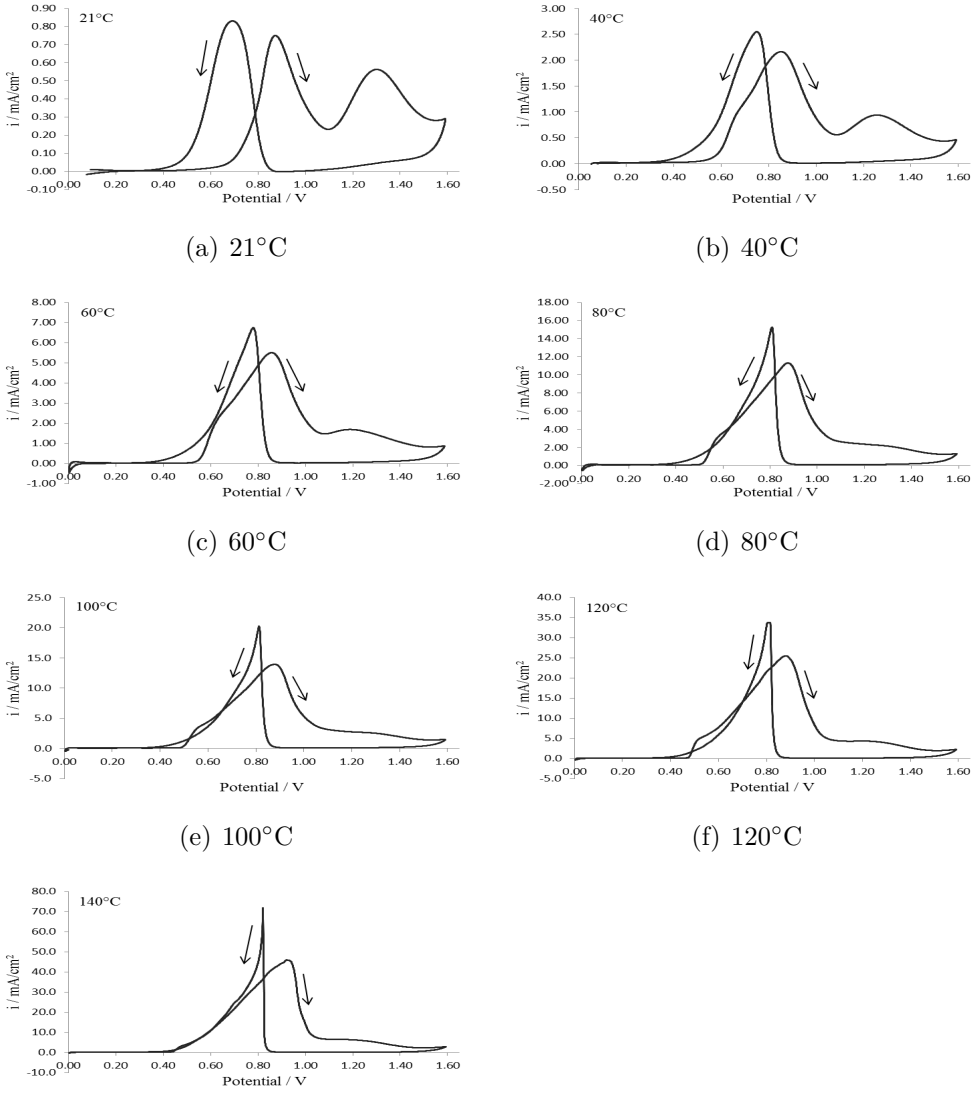

(a) 21°C

(b) 40°C

(c) 60°C

(d) 80°C

(e) 100°C

(f) 120°C

(g) 140°C

Figure 5.16: Cyclic voltammograms acquired while performing dEIS measurements for 0.2 M ethanol in 0.5 M sulphuric acid at different temperatures with 10 mV/s sweep rate

The cyclic voltammograms that were recorded while doing dEIS measurements are given in Figure 5.16. They show the same trends for changes in the cyclic voltammogram with temperature as the voltammograms for ethanol with 100 mV/s sweep rate given in Figure 5.10. One feature that can be observed here that is not as clearly visible in the voltamograms with 100 mV/s is that there is a fast increase in the current density at the start of the first peak for temperatures from 40°C.

Selected electrochemical impedance spectra registered when doing dynamic electrochemical impedance spectroscopy at 60°C with 1 mV/s sweep rate are given in Figure 5.17 together with the underlying d.c. voltammogram by way of comparison.

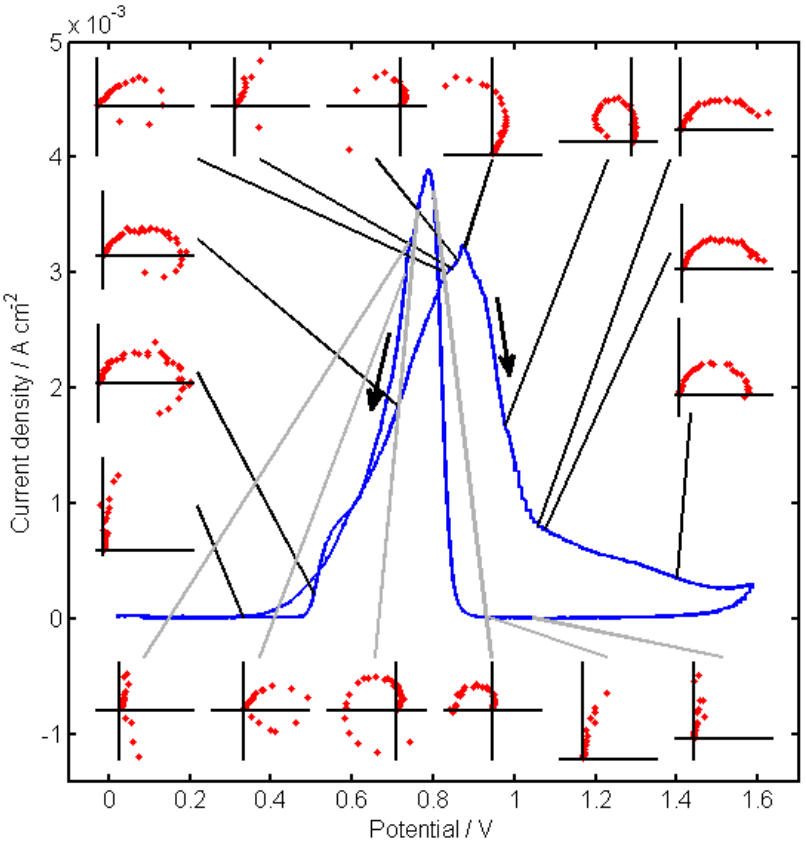

Figure 5.17: Summary of EIS behaviour for 200 mM ethanol on a platinum surface in 0.5 M sulphuric acid at 60°C with 1 mV/s sweep rate

Observations that can be made from Figure 5.17 is that there seem to be a lot of changes in the impedance behaviour of the system in the potential region around the first oxidation peak in positive scan direction, approximately 0.8-1.1 V. The

impedance behaviour in the region between 0.4 and 1 V in the positive scan direction seem to be more complicated than the impedance behaviour below 0.4 V and 1 V. The impedance behaviour in the negative scan direction also seem more complicated in the region between 0.4 and 0.9 V. Impedance behaviour that was registered while doing dynamic electrochemical impedance spectroscopy (dEIS) does not seem to be the same in the positive and reverse scan.

Similar summaries of the impedance behaviour observed for 5 and 10 mV/s sweep rate for 0.2 M ethanol and 60°C are given in Appendix B. One observation that can be made from Figure 5.18 is that there is small differences between the Nyquist diagram when the sweep rate of the "d.c."-potential changes. This difference is mainly in the size of the values of the real and imaginary parts. The shape of the spectra were visually the same and resembled the same features.

Figure 5.18 shows how the Nyquist plots for 700 mV at 60°C changes with changing sweep rate.

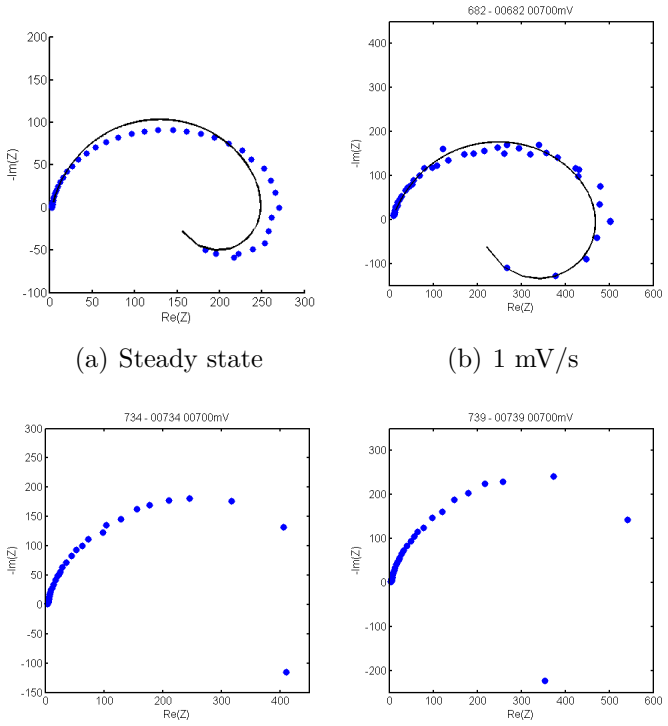

(a) Steady state (b) 1 mV/s

(c) 5 mV/s (d) 10 mV/s

Figure 5.18: Nyquist plots acquired while doing dEIS for 700 mV at 60°C for (a) steady state and (b) 1, (c) 5 and (d) 10 mV/s sweep rate

The EIS spectra for the dEIS measurements at 60°C with sweep rate of 1 mV/s was fitted to equivalent circuits. The equivalent circuits that are used for fitting the data are given in Figure 5.19.

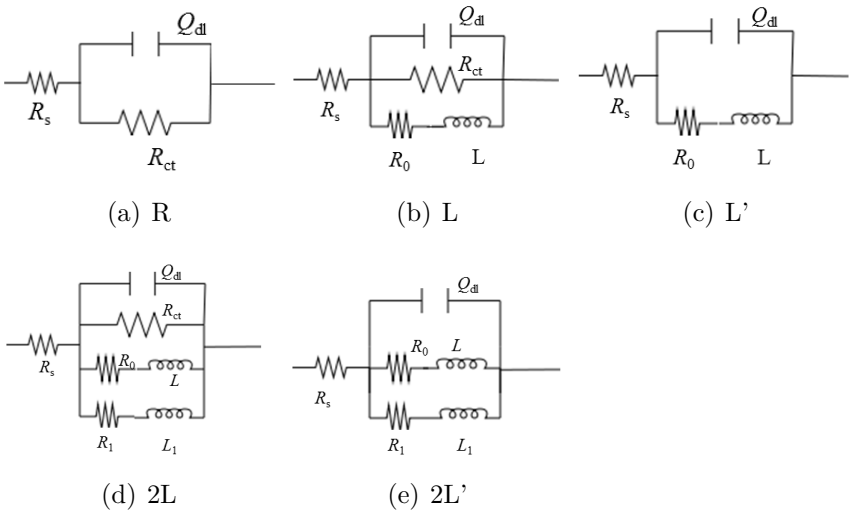

(a) R (b) L (c) L'

(d) 2L (e) 2L'

Figure 5.19: Equivalent circuits used for fitting of results

The summary of the fitting results is given in Table 5.2. The fitting was validated by use of F-test for addition of an additional element. It is worth noting that there were some noise influencing the 2.2 kHz frequency.

Table 5.2: Summary of fitting results for 60°C with 1 mV/s sweep rate

Potential Region	Circuit	Sign of R_0	Sign of L	Sign of τ
0.520-0.840 up	L[1]	+	+	+
0.841-0.844 up	L'	+	+	+
0.860-0.930 up	L'	–	–	+
0.940-1.000 up	L	–	–	+
1.010-1.030 up	L'	–	–	+
1.040 up	L	–	–	+
1.050-1.600 up	R	n/a	n/a	n/a
1.600-0.840 down	R	n/a	n/a	n/a
0.838-0.794 down	L	–	–	+
0.792-0.750 down	2L	–	–	+
0.736-0.704 down	L	+	+	+
0.702-0.350 down	R	n/a	n/a	n/a

[1] Circuit R was the better fit according to the F-test, but circuit L was the best fit when visually inspecting the EIS spectra including the fitted line.

In the potential region 0.500-0.590 the fitting of data and validation using F-test suggested that R was the best circuit, but from visually inspecting the eis spectra L should be the best fit. This was due to low errorbars on some parameters and an unrealistic high errorbar on one of the parameter when using the circuit R. There was also some difficulty fitting the results to equivalent circuits in the area around the peak, at the potential region 0.830-0.860.

The best fit in the potential regions 0.841-0.844 V and 0.860-0.910 V in the forward scan was obtained by using circuit L where the charge transfer resistance had been removed, circuit L'. There is no reason for neglecting the charge transfer resistance other than it is most probably undetectable in the fitting routine used. This may be due to either very large value of R_{ct} existing as a small curvature in the CPE region, or a low value of R_{ct} hidden in the high frequency region [29].

The charge transfer resistance, R_{ct} was calculated as part of the fitting of electrochemical impedance spectroscopy data obtained at 60°C. The results of this is shown in Figure 5.20. This figure shows that the charge transfer resistance calculated is decreasing from approximately 6.9 kΩ at 0.36 V to 480 Ω at 0.7 V for both negative and positive going scan. In the potential region between 0.84 V and 1.03 V there are no calculated values in the positive going scan, because the best fitting of data was obtained by using circuit L' (Figure 5.19 (c)). The charge transfer resistance was between 350 Ω and 760 Ω in the potential region

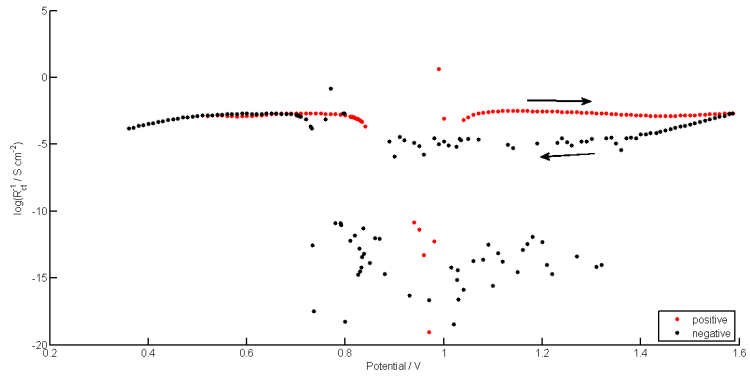

Figure 5.20: Potential variations of charge transfer resistance, R_{ct}, calculated from fitting of data obtained doing dynamic electrochemical impedance spectroscopy at 60°C with sweep rate 1 mV/s

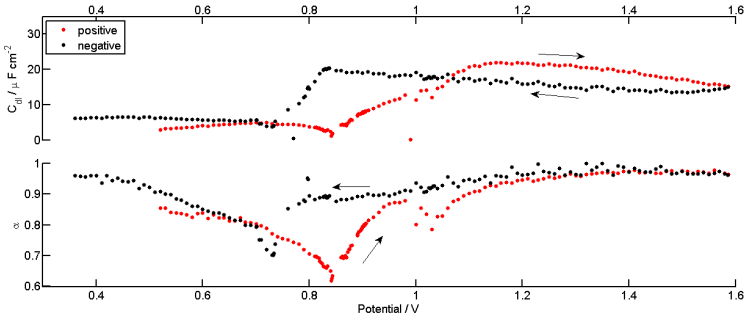

Figure 5.21: (a) Potential dependence of capacitance and (b) values of the CPE exponent, α, calculated from impedance data at 60°C and sweep rate 1 mV/s

between 1.03 V and 1.6 V in the positive going scan. For the reverse scan there is an increase in R_{ct} when the potential is changed from 1.6 V to 0.90 V from 760 Ω at 1.6 V to 0.83 MΩ when the potential is 0.90 V.

The capacitance was also calculated as a part of the fitting of the electrochemical impedance data. The results of this is shown in Figure 5.21. This figure shows that there is an increase in the capacitance at approximately 0.8 V in the forward scan and that there is a decrease in the capacitance at approximately the same potential for the negative scan. When comparing Figure 5.21 and Figure 5.15 (f) it is possible to see that these figures show the same trends, as would be expected as the admittance of the imaginary part at these frequencies is essentially only the double layer capacitance.

Polarisation resistance R_p was calculated from the values of the fitted data from

dEIS measurements at 60°C with 1 mV/s sweep rate and estimated from the cyclic voltammetry curve at the same temperature and sweep rate and compared with each other. To estimate polarisation resistance from the cyclic voltammetry curve (low sweep rate) the following relationship was used

$$\frac{1}{R_p} = \frac{\mathrm{d}j_{ss}}{\mathrm{d}E_{ss}} \tag{5.2}$$

, where R_p is the polarisation resistance, j_{ss} is the steady state current and E_{ss} is the steady state potential. The following relationship was used for calculation of the polarisation resistance from the values of the fitted data from dEIS measurements

$$Rp = Z(\omega \to 0) \tag{5.3}$$

Where R_p is the polarisation resistance, Z is the impedance and ω is the angular frequency.

The results of the calculations of R_p is shown in Figure 5.22. The diamonds show the values calculated from the cyclic voltammogram and the squares show the values calculated from the fitted parameters from the dEIS measurements.

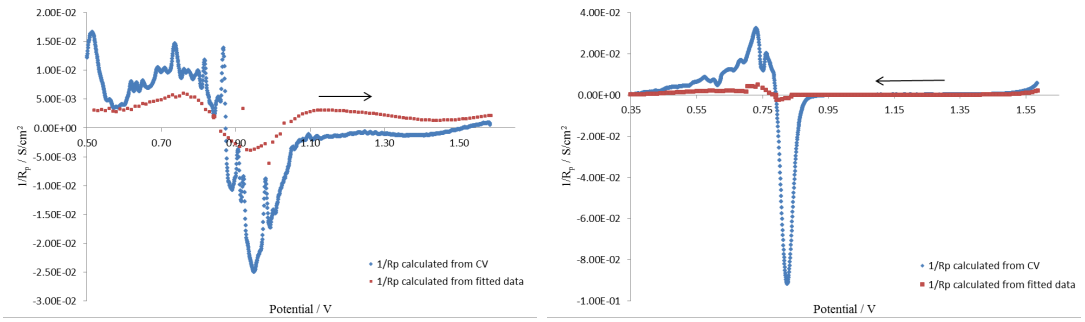

(a) (b)

Figure 5.22: Changes in $1/R_p$ with potential in (a) the positive scan direction and (b) negative scan direction for 60°C with 1 mV/s sweep rate

5.3.1 Effect of temperature

Figure 5.24 shows how the Nyquist plot changes with changing temperature for potentials of approximately 700 mV when doing dynamic electrochemical impedance spectroscopy. An interesting observation that can be made from Figure 5.24 is that some impedance values in the Nyquist representation obtained for 700 mV at room temperature (Figure 5.24 (a)) crosses into the second quadrant. One point is even observed in the third quadrant, although low frequency values may be inaccurate.

The changes in the charge transfer resistance with temperature in the potential region 0.5-0.7 V is shown in Figure 5.23. The charge transfer resistance was calculated by fitting EIS spectra in the region 0.5-0.7 V to circuit R by use of ZSimpWin with modulus weighting. It was necessary to fit the spectra to a more complicated circuit, L, in the potential region 0.64-0.7 for room temperature. An observation that can be made from this figure is that the charge transfer resistance decreases with increasing temperature.

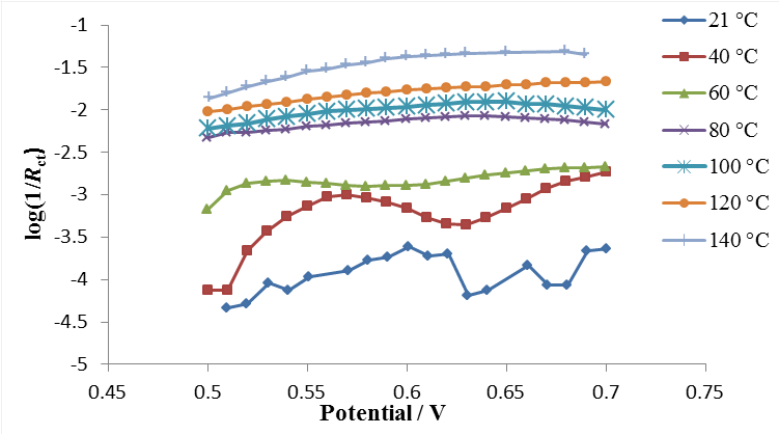

Figure 5.23: Charge transfer resistance, R_{ct} for the different temperatures is plotted versus potential in the potential region 0.5-0.7 V

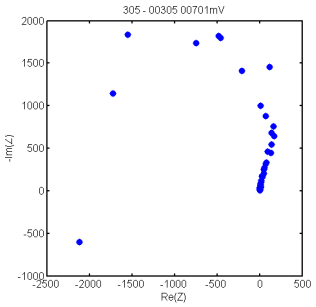

(a) 21°C

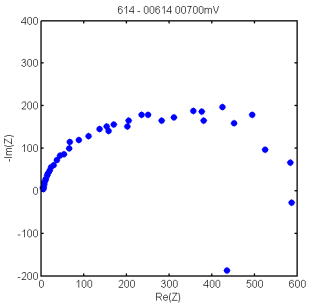

(b) 40°C

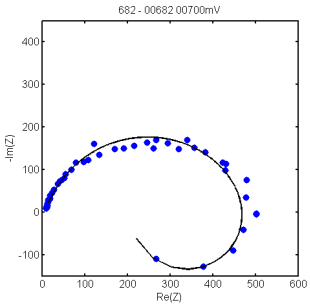

(c) 60°C

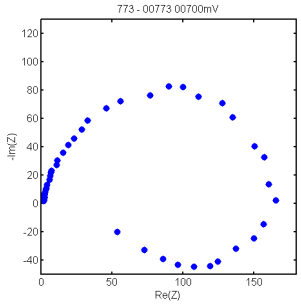

(d) 80°C

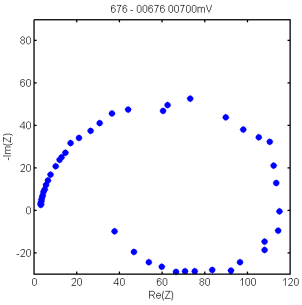

(e) 100°C

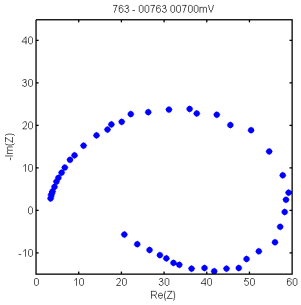

(f) 120°C

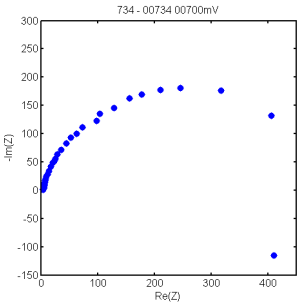

(g) 140°C

Figure 5.24: Nyquist plots acquired while doing dEIS for 0.2 M ethanol at approximately 700 mV at different temperatures with 1 mV/s sweep rate

6 Discussion

6.1 DC measurements

6.1.1 Blank Solution, 0.5 M Sulphuric Acid

One observation that was made from the results of cyclic voltammetry for blank solution with varying temperatures was that there were some differences in the oxide region when the temperature changed. Figure 5.2 shows that there is a negative shift of the potential where platinum oxide formation is initiated with increasing temperature. This is most likely due to thermal activation of water adsorption, as discussed by Behm and Jusys, and Bokach et al. [30, 31]. Temperature effects of Pt oxide formation was first shown recently up to 50°C by Alsabet et al. [32], and up to 70°C by Cohen et al. [33]. In this work it is given up to 140°C tracing the same trends as shown previously. The current density for platinum oxidation and oxygen production is also increasing with increasing temperatures. These observations indicate that the reaction rates of formation and reduction of platinum oxide increases with temperature.

It is also possible to see that the curve around the onset of oxidation of platinum gets steeper when the temperature increases. This is due to increased kinetics at the elevated temperatures [34]. Another effect that it is possible to see from the figure is that there is an increase in peak potential for reduction of platinum with increasing temperatures. These findings corresponds to what Cohen et al. (2007) and Alsabet et al. (2006) observed for platinum in H_2SO_4 when temperature increased [33, 32].

6.1.2 Carbon monoxide, CO

In Section 5.1.2 the results from cyclic voltammetry in combination with rotating disk electrode (RDE) is given. CO adsorbs readily at the Pt electrode and blocks all surface sites, which can be seen from the lack of current in the hydrogen region. As the potential is increased there is no CO-stripping until well into the potential of oxide formation. Oxide formation seem impeded by the compact CO(ads) layer formed during potential sweep at lower potentials, this shifts the onset of CO-oxidation to more positive potentials. CO strips off in a sharp peak for lower scan rates while for higher scan rates there are not enough time for a complete adsorption of a CO monolayer which leads to a less sharp peak [28].

Furthermore, it is possible to see that the oxidation of CO on a Pt-electrode seems

to be controlled by mass transfer. This can be further emphasised by looking at a Levich-plot for CO oxidation (Figure 5.5). As it is possible to see from Figure 5.5 the plot of current density versus the square root of the rotation speed is approximately forming a straight line going through origin. This suggests that CO oxidation of on Pt-electrodes is diffusion controlled.

6.1.3 Ethanol

Some results of cyclic voltammetry with ethanol in 0.5 M sulphuric acid is presented in Section 5.1.3. From these results it is possible to see that there is a certain connection between the cyclic voltammogram of platinum in acidic solution and ethanol in 0.5 M sulphuric acid on platinum surface. There seems to be an increase in the current for ethanol oxidation in the same region as the onset of platinum oxidation. It is also possible to see that there is a connection between the potential for reduction of platinum oxide and the oxidation peak for the reverse scan. This indicates that there is a connection between oxidation of platinum and the oxidation of ethanol. This supports the assumption that water or adsorbed water species is necessary for the oxidation of ethanol. Lamy et al. (2002) concluded that reaction mechanism for alcohol oxidation always involves the participation of water or its adsorption residue [1].

When comparing the voltammogram for ethanol with the voltammogram for CO-stripping it is possible to see that there is an increase in the current at lower potentials (0.55 V) for ethanol than for CO (0.90 V) with sweep rate 100 mV/s at 21°C. Ethanol requires several neighbouring surface sites in order to interact with the surface. Thus a complete adsorbed layer of surface-bound poisoning species is not possible, and ethanol oxidation may be initiated at potentials lower than the case for dissolved CO(aq).

However, the cyclic voltammograms of ethanol in acid shows an apparent complete blocking at low potentials as the current is low. The platinum surface seems to be completely blocked by a surface adsorbed poisoning species until the potential where the first oxidation peak starts in positive-going scan direction.

Cyclic voltammetry of ethanol with different concentrations of ethanol showed differences as the concentration changed. There was an increase in the current density of both oxidation peaks in the positive scan direction and the oxidation peak in negative scan direction with increasing ethanol concentration. The peak potential for the first oxidation peak increased from 0.85 V to 0.95 V when the ethanol concentration was increased from 0.01 M to 1 M. This indicates that it is necessary to increase the potential more to reach the optimal surface condition

for oxidation in the first peak when the concentration increases. There is a decrease in the peak potential for the second peak from 1.35 V to 1.27 V when the concentration is increased from 0.01 M to 1 M. This indicates that the optimal surface condition is reached at a lower potential for the oxidation reactions in the second surface peak when the concentration of ethanol is increased. Another change in the voltammograms with increasing ethanol concentration was that the anodic peak that corresponds to reduction of platinum oxide decreased with increasing concentrations of ethanol. This may be an effect of that it is easier to get enough ethanol on the surface to facilitate the oxidation at higher concentrations. It is less need for platinum reduction prior to oxidation of ethanol.

6.1.4 Effect of Temperature on Ethanol Oxidation

Temperature effects on ethanol oxidation that can be seen from d.c. measurements done in this work is that there is an increase in current density for the first oxidation peak with increasing temperatures. The peak current density for the second peak is also increasing with increasing temperatures, but it is increasing less than the current density for the first peak. At the highest temperatures it is hard to see that the second peak is a peak at all, it looks more like a plateau. This can be an indication that the reaction kinetics for the reactions happening in the second oxidation peak is slower than the reaction kinetics for the first peak.

Another interesting feature that can be seen from the voltammograms for ethanol with sweep rate 100 mV/s as the temperature increased is that there is a shoulder in the start of the first peak at higher temperatures. This shoulder is not visible in the voltammogram at room temperature. Furthermore, this shoulder seems to appear at lower potentials as the temperature increases. This shoulder can indicate that there are two different reactions occurring at different potentials during the first peak. For example, if the main peak is related to Pt oxide formation and the optimum surface condition with ethanol activity, the shoulder could be related to some sort of surface-bonded water at lower potentials. Thermal enhanced water adsorption could explain the shift towards more negative potentials for this shoulder.

The onset potential for the first oxidation peak decreases when the temperature increases. This shows that there seem to be an overpotential decrease when the temperature increases. This decrease in overpotential can come from increased water activity at the surface at higher temperatures. That there seem to be results indicating a decrease in overpotential for ethanol fuel cells at higher temperatures suggest that it seem favourable to operate ethanol fuel cells at higher temperatures than ambient to get a better effect.

The oxidation peak in the reverse scan gets increasingly steep as the temperatures increases and at the highest temperatures used in this work it is almost perpendicular. And the peak potential increases with increasing temperatures, but stabilises at approximately 0.8 V, this corresponds with the change of peak potential for platinum oxide reduction for platinum in sulphuric acid with increasing temperatures. Even though Pt oxide shows high degree of irreversibility at all temperatures, there is a significant increase in the reaction rate for ethanol oxidation at freshly reduced Pt surface. Once the Pt oxide is being reduced, the ethanol adsorbs and oxidises immediately in great quantities.

The apparent activation energy E_A was calculated at the potentials; 0.5, 0.6, 0.7 and 0.8 V. There was seen a trend where the activation energy decreased with increasing potentials. This can be connected to the changes in the voltammograms with temperature. The activation energy was largest in the areas where the current changed most with temperature changes. This indicates that the largest change in the current with increasing temperatures is for the lowest potentials. The reaction in this area seem dependent on a higher temperature in order to happen. There is of course some uncertainty connected with the calculated activation energies, which means that the calculated values may not be exact. There is always some error when doing linear regression and this will of propagate to the calculation of the activation energies. When doing experimental work there will almost always exist experimental errors which also will affect the calculation of activation energy.

6.1.5 Different Upper Limits

Cyclic voltammetry with different reversal potentials were done for blank solution, 0.5 M sulphuric acid, at room temperature and for 0.2 M ethanol in 0.5 M H_2SO_4 at different temperatures. From the results for 0.5 M sulphuric acid it is possible to see that the onset potential for reduction of the platinum oxide is more positive when the upper limit for the cyclic voltammetry is reduced. This suggests that it is easier to reduce platinum oxide when the upper limits of the cyclic voltammetry have been reduced. From the shape of the voltammograms it also looks like the oxidation reaction of platinum is more reversible when the reversal potentials were lower. Possible explanations for this can be that the oxide is looser bonded when the oxidation reaction of platinum have occurred at lower potentials or that there is a rearranging of the surface that occurs at high potentials. This is also in accordance with what some other studies on platinum oxide growth have found [35].

Cyclic voltammetry of 0.2 M ethanol with different upper limit showed that the oxidation peak in the reverse scan direction have a higher onset potential as the upper limits for the voltammetry was decreased. This trend was observed at all

temperatures. This seems to be related to the higher onset potential for platinum reduction with lower reversal potentials in blank solution. This suggests that the oxidation reaction that occurs in the peak in the reverse scan occurs easier when the platinum oxidation reaction is occurring at higher potentials due to easier reduction of platinum oxide.

6.2 AC measurements

6.2.1 AC Voltammetry

Selected AC voltammograms for dynamic electrochemical impedance spectroscopy measurement done at 60°C with 1 mV/s sweep rate were shown in Section 5.2.

An observation that can be made from Figure 5.15 is where the real or imaginary admittance goes through zero. When the real part of the admittance becomes negative it is usual to observe that the spectra are moving into the second or third quadrant. A negative imaginary admittance will indicate that the spectra are moving into the third or fourth quadrant [29].

The imaginary part of the admittance for higher frequencies largely represents the double layer capacitance. From a look at Figure 5.15 (f), the imaginary part of the admittance at 104 Hz, it is possible to see that it is expected an increase in the double layer capacitance at approximately 800 mV. It is also possible to see that there is an expected decrease in the double layer capacitance at approximately 800 mV for the reverse scan direction. The increase happens at the potential where the oxidation of platinum is expected to start. This indicates that the formation of platinum oxide have an influence on the double layer capacitance.

When comparing Figure 5.15 (f) with the values for the double layer capacitance that was calculated by fitting of the impedance spectra to some selected circuits shown in Figure 5.21 it is possible to see that the capacitance of the double layer is increasing and decreasing at the same potentials as the imaginary part of the admittance at 104 Hz. This gives a confirmation that the values of the capacitance that is calculated by the fitting of EIS spectra seem reasonable.

6.2.2 Electrochemical Impedance Spectroscopy

Dynamic electrochemical impedance measurements (dEIS) were done at different temperatures with sweep rates of 1, 5 and 10 mV/s. The discussion around the results from these experiments will mainly focus on the results from the

measurements at 60°C with sweep rate of 1 mV/s. But some discussion will also be given around the differences between experiments with sweep rates 1, 5, and 10 mV/s at 60°C and for sweep rate 1 mV/s at different temperatures.

A fitting of the data from dEIS measurements at 60°C with sweep rate of 1 mV/s was done. The results from this fitting is summarized in Table 5.2, and Figure 5.19 gives a visual presentation of the circuits that was used for the fitting. The reason for the circuit choices was that it is possible to link these circuits to possible surface processes at platinum for ethanol electro-oxidation. Circuit R is often related to simple electrochemical reactions. Circuit L is associated with reactions with two time constants, which as an example can be a reaction with two species at the surface. And circuit 2L is associated with reactions with three time constants; this can be a reaction with three species on the surface [11]. L' and 2L' were used in some potential regions in order to get an improved fit with realistic error bars. This does not mean that the there is no charge transfer resistance, R_{ct}, it is probably because the value of R_{ct} was either too small or too large to get a good fitting when this was present in the circuit[29].

The results of the fitting of the dEIS measurements at 60°C with 1 mV/s sweep rate suggests that the reaction or reactions occurring on the surface in the potential region between 0.52 V and 1.04 V consists of one independent species and one time constant related to adsorption. In the potential region between 1.04 V and 1.6 V the results from fitting of data suggest that the surface is entirely covered with one species, which probably is oxide.

For the negative going scan the results suggests that the reaction occurring in the potential regions 0.838-0.794 V and 0.736-0.704 V is also consisting of one kinetically significant species. For the potential region 0.79-0.750, in a potential region where the slope of the polarization curve indicates positive polarization resistance, second (and third) quadrant behaviour was seen. One extra time constant is needed to explain third quadrant behaviour. For this potential region the surface is probably described by coverage of two independent species.

Dynamic electrochemical impedance spectroscopy was done at different temperatures. Figure 5.24 shows how the impedance behaviour changed with temperature at 700 mV when the sweep rate was 1 mV/s. One feature that can be seen from this figure is that there seemed to be more noise in dEIS measurements carried out at lower temperatures. It is also possible to see that there is a large difference between the Nyquist diagram at room temperature and the Nyquist diagrams for higher temperatures. In the Nyquist diagram at room temperature it is possible to see that the impedance response is showing both second and third quadrant behaviour, this is something one might expect when the slope of

the voltammogram is negative, but the slope of the voltammogram at 700 mV is positive. This indicates that we have hidden negative differential response (HNDR), which can indicate an instability in the oxidation process. There is also a difference in the spectrum for 40°C at 700 mV from the other spectra. The half-circle in the first quadrant is very long at this temperature, this is different from the other temperatures. The other temperatures show Nyquist diagrams that are similar to each other with first and third quadrant behaviour and increasing values for increasing temperatures.

A plot of the changes in charge transfer resistance, R_{ct} with potential is given in Figure 5.20. This figure shows that there is a decrease in the charge transfer resistance when the potential increases up to 0.8 V in positive going scan. This figure also shows that there is an increase in the charge transfer resistance when doing negative sweep from 1.6 to 0.9 V. This can be due to a build-up of the oxide layer on the surface in this region. Another feature that it is possible to see from this figure is that there is some charge transfer resistances that is really high in potential regions where other fitted values from the data is smaller. This is an indication that the fitting of data in this region is not optimal.

Changes in charge transfer resistance with temperature is given in Figure 5.23 from these results it is possible to see that the charge transfer resistance decreases with temperature. This can be an indication of better reaction kinetics with increased temperature. From this figure it is also possible to see that there is some differences in how the charge transfer resistance, R_{ct} changes with potential. For the highest temperatures, 60-140°C, the changes with potential seem quite similar, but there is a difference in the changes with potential for the two lowest temperatures, 21°C and 40°C. This can suggest that there are some changes in the surface reactions when the temperature increases.

A comparison of polarisation resistance, R_p, calculated from the cyclic voltammogram with 1 mV/s sweep rate at 60°C and from the parameters found by fitting dEIS data from the same temperature and sweep rate is given in Figure 5.22. This figure shows how $1/R_p$ changes when the potential changes. This figure shows that it is a good correlation between the polarisation resistances calculated from fitted dEIS data and from the cyclic voltammogram in the potential regions between 0.52 and 1.0 V in the positive scan direction. For the potential region 1.0-1.5 V the sign for the polarisation resistance calculated from the cyclic voltammogram and from the fitting of the dEIS data does not have the same sign, which may suggest that the dEIS measurements did not manage to pick up all information about the reactions in this area. This indicates that there is at least on relaxation missing in this potential region. From 1.5 to 1.6 V the values for R_p have the same sign again and the EIS data seem to have picked up all information about

the reactions.

For the negative going scan direction there seem to be a good correlation between the polarisation resistances calculated from CV and from dEIS at potentials below 0.6 V and above 0.95 V.

Some areas where the polarisation resistance seem to be different in size when calculated by the two different methods are corresponding to areas where the current seem to change a lot. This is in accordance with the theoretical limitations of time resolved Fourier transform electrochemical impedance spectroscopy (FFT-EIS) given by Garland, Pettit and Roy (2004) [16]. They found that a theoretical constraint for FFT-EIS is that the change in the d.c. current, $\bar{j}$ is much smaller than the changes in the a.c. frequency for the smallest frequency, $\tilde{j}(f_{min})$ as given in the following equation

$$\left|\frac{\mathrm{d}\bar{j}}{\mathrm{d}t}\right| = \left[\frac{\mathrm{d}}{dt}\{\tilde{j}(f_{min})\}\right]_{rms} \tag{6.1}$$

Where f_{min} is the minimum frquency and t is the time.

According to Lasia (1999) electrochemical impedance spectroscopy is a very sensitive method and must be used caution. EIS does not provide direct measurement of physical data and should be used in combination with other methods, as dc methods or transients, and with good physical knowledge of the system [13]. In this work cyclic voltammetry with different sweep rates and different upper limits was done in addition to EIS measurements to give a better understanding of the system and reactions.

Another danger when doing graphical fitting to equivalent circuits is that addition of an additional term will in most cases lead to a better fit to the curve, lower χ^2 value. This can lead to selection of a too complicated model even when the data from the fitting does not give a complicated spectrum. One way to avoid this is to use the F-test for addition of an additional term [27] to confirm that it is correct to use a more complicated circuit. This has been done in this work with one exception. For the potential region 0.52-0.84 V in positive going scan L was not confirmed as the best fit with a likelihood of 1% to be wrong. According to the F-test circuit R should have been chosen in this potential region, but from visual examination of the spectra it was possible to see that it was observed fourth quadrant behaviour. Circuit R is not adequate to describe this behaviour, it is necessary with at least two time-constants to describe fourth quadrant behaviour properly.

6.3 Instabilities in oxidation processes

EIS spectra indicate regions where instabilities may occur during the electro-oxidation. This could be seen from the Nyquist diagram for 700 mV at 21°C given in Figure 5.24 (a) and from the summary of the dEIS measurements at 60°C with 1 mV/s sweep rate given in Figure 5.17. Regions of negative impedance values in the positive slope of the polarization curve are commonly referred to as "hidden" negative differential resistance (HNDR).

According to Krischer and Varela a characteristic feature for electrochemical oscillations is that the potential is an essential parameter [36]. The observed instability looks like a Hopf bifurcation as classified by Koper et al. (1996) [37]. A Hopf bifurcation can lead to current oscillations if large enough ohmic resistance is added to the working electrode circuit translating the impedance spectra to more positive real values and eventually through origin. Hidden negative resistance can be seen as a system composed of a subsystem with a N-shaped stationary curve where the negative slope is hidden by another slow and potential dependent step of the interfacial kinetics of the entire system. The slow step dominates at low frequencies of perturbations, while the fast subsystem dominates at higher frequencies. The slow step is often adsorption of blocking species at the surface [36]. Hidden negative differential resistance have also been observed for formic acid and methanol [34].

6.4 Reaction Mechanism for Ethanol Oxidation

In this section it is going to be given a suggested simplified reaction mechanism for ethanol oxidation on platinum surfaces on the basis of the results of the experiments done as a part of this work and existing literature regarding ethanol oxidation.

The results of fitting of the dynamic electrochemical impedance spectroscopy data for 1 mV/s sweep rate at 60°C is given in 5.2. These results suggest that the surface is completely described by one kinetically significant species for potentials between 0.52 and 1.04 V in the positive going scan. The results from the dEIS measurements at 60°C also indicates that this is the case in the potential region between 1.05 and 1.60 V in the same scan direction.

In the negative scan direction it looks like the surface can be described by one surface state between 1.60 down to 0.794 V, in the potential region between 0.838 and 0.794 V the surface again seem to be covered by one kinetically significant species. But the region between 0.792 and 0.750 V is described by one additional

time-constant and there is a need for an extra kinetically significant species to fully describe the surface. In the region between 0.734 and 0.704 V the region again seem to be covered by one independent species. For the potentials below 0.702 V the surface seem to be entirely covered with one species.

The work presented in this thesis have not looked into which species that is detected on the surface and it is therefore necessary to use other literature regarding ethanol oxidation to get an understanding of which adsorbed species that it is likely to find on the platinum surface under the conditions for dEIS measurements at 60°C. Sun et al. (2009) did a study of ethanol electro-oxidation at a Pt/C-catalyst at elevated temperature and pressure by DEMS. This study found that CO_2 was only a minor product when doing cyclic voltammetry at 60°C with a concentration of 0.1 M ethanol and 10 mV/s sweep rate the maximum CO_2 current efficiency found was 5%. The CO_2 current efficiency found for steady state experiments at 60°C for 0.1 M ethanol and 0.01 M ethanol was found to be 9.8 and 26.8% respectively [24]. The concentration used in this experiment was 0.2 M and from the results of the study done by Sun et al. the expected CO_2 current efficiency is even smaller than 5%. This indicates that one of the adsorbed species at the platinum surface in the potential regions with one kinetically significant species is most likely dominated by another species than CO(ads).

From other studies on ethanol electro-oxidation it is possible to see that two common side products are acetaldehyde and acetic acid [6, 20, 4]. A study done by Hitmi et al. in 1994 gave results indicating that acetaldehyde was the main product in the potential region up to 0.8 V [20]. In a study by Wang, Jusys and Behm (2004), where ethanol oxidation was studied by DEMS, it was seen that both acetic acid and acetaldehyde are products of the ethanol electro-oxidation [6].

Vigier et al. (2004) did a study of the electro-oxidation of ethanol by electrochemical methods and in situ IR reflectance spectroscopy. This study suggests two possible adsorbed species carbon monoxide, CO and acetyl, $COCH_3$ [4]. This suggests that one of the adsorbed species on the surface in the potential region between 0.52 and 1.04 V can be acetyl.

The other adsorbed species on the surface is probably one form of adsorbed water or water derivative. This is because the oxidation of ethanol to both acetic acid and CO_2 cannot happen without water or adsorbed water residues (for example adsorbed OH) [2].

From the results of the cyclic voltammogram acquired simultaneously with dEIS measurements at 60°C and sweep rate 1 mV/s it seems like the surface is completely blocked by a surface adsorbed species until the potential on the surface is approximately 0.45 V. This surface adsorbed species is most likely an

adsorbed ethanol residue. At the potentials above 1.05 V the surface is most likely completely covered with platinum oxide. The current that was observed in the CV together with the results from the fitting of the dEIS data for the potential region between 1.6 and 0.84 V suggests that the surface is completely covered with one species that inhibits further reaction, probably platinum oxide.

In the potential region between 0.84 and 0.794 V the results from the EIS suggests that the surface is covered by two species, i.e. one kinetically significant species. This can be acetyl as assumed in the positive scan direction, or acetate. But in a study by Heinen, Jusys and Behm (2010) of oxidation of ethanol, acetaldehyde and acetic acid the results indicated that one adsorbed intermediate that is present in the reverse scan direction in the potential region between 0.8 and 0.4 V is adsorbed acetate [38]. Acetate is not expected to oxidise further. The current increase is therefore not likely to come from oxidation of acetate and the adsorbed intermediate that is detected in the dEIS measurements is therefore more likely to be acetyl.

One observation that was made in the negative going scan direction and not in the positive direction is that the dEIS results suggests the presence of hidden negative differential resistance and two independent species at the surface for one small potential region. This is observed for potentials between 0.792 and 0.750 V. As for the other potentials two of the species at the surface is probably oxide or water and acetyl. The last species can be adsorbed CO which is a species observed during ethanol electro-oxidation [4, 24], adsorbed acetate [38], or bare Pt sites. The CO_2 current efficiency that Sun et al. found for the same potential region at 60°C with sweep rate of 10 mV/s was around 5% [24], this is very low and can be an indication that the species that is adsorbed is not adsorbed CO but another species. The other adsorbed species can from these studies seems to be acetate.

In the potential region between 0.736 and 0.704 V the results from the dEIS measurements indicates only kinetically significant species at the surface. One species at the surface in this region is likely to be platinum with loosely bonded water as for the surface in the same potential region in the positive going scan. The second species is probably acetyl which can desorb and form acetaldehyde or react further and form acetic acid. From the results of the dEIS measurements and the simultaneously acquired cyclic voltammograms the surface seem to be entirely covered with one species at potentials lower than 0.702 V. And at potentials lower than 0.35 V the surface is completely blocked by a surface adsorbed species.

In the study by Heinen, Jusys and Behm (2010) they found a difference between ethanol oxidation and oxidation of acetic acid. Furthermore, they suggest that the ethanol oxidation seem to be reversible adsorption of acetate on the platinum

surface [38].

A simplified reaction mechanism is made on background of the foregoing discussion, and the following assumptions have been made. The reaction of an adsorbed species which leads to acetaldehyde is fast and this adsorbed intermediate have not been registered on the surface during this experiment. The rate of formation of CO(ads) is so low that it is not possible to register CO(ads) as a surface adsorbed species, the surface adsorbed blocking species for potentials below 0.5 V is a surface adsorbed ethanol derivative.

For potentials below 0.5 V the surface is completely covered by acetate which is blocking other reactions:

$$\mathrm{Pt{-}CH_3COO} \tag{6.2}$$

In the potential region between 0.52 and 1.040 V the surface is covered with two species, one is kinetically significant. The surface species is assumed to be some form of adsorbed water derivative, as an example OH (Equation 6.3) and acetyl. Acetyl can come from readsorption of acetaldehyde and ethanol. The chemical equations for these reactions is given in Equation 6.3 to Equation 6.7.

$$\mathrm{H_2O + Pt \longrightarrow Pt{-}OH + H^+ + e^-} \tag{6.3}$$

$$\mathrm{2H_2O + Pt \longrightarrow Pt{-}O + 2H^+ + 2e^-} \tag{6.4}$$

$$\mathrm{CH_3CH_2OH + Pt \longrightarrow Pt{-}COCH_3 + 3e^-} \tag{6.5}$$

$$\mathrm{CH_3CHO + Pt \longrightarrow Pt{-}COCH_3 + 1e^-} \tag{6.6}$$

$$\mathrm{Pt{-}OH + Pt{-}COCH_3 \longrightarrow CH_3COOH + 2Pt + 1H^+ + 1e^-} \tag{6.7}$$

For the positive going scan the surface seem to be blocked for further oxidation at potentials over 1.050 V due to complete covering by oxide. The same is seen for potentials above 0.84 V in the negative going scan direction.

$$\mathrm{H_2O + Pt \longleftarrow Pt{-}O + 2H^+ + 2e^-} \tag{6.8}$$

In the potential regions 0.838-0.79 and 0.736-0.704 V in the negative going scan the surface also seem covered by one independent species and the reaction is probably

following the same equations as for the potential region between 0.52 and 1.040 V in the positive going scan as described by Equation 6.3 to Equation 6.7.

There is one potential region in the negative going sweep where the results indicate that the surface is covered by two independent species. In this region it is assumed that the reactions are given by the following equations. Where the reaction given by Equation 6.13 can be the reaction giving the negative feedback loop creating HNDR.

$$CH_3CH_2OH + Pt \longrightarrow Pt{-}COCH_3 + 3e^- \tag{6.9}$$

$$CH_3CHO + Pt \longrightarrow Pt{-}COCH_3 + 1e^- \tag{6.10}$$

$$Pt{-}OH + Pt{-}COCH_3 \longrightarrow CH_3COOH + 2Pt + 1H^+ + 1e^- \tag{6.11}$$

$$Pt + CH_3COOH \longrightarrow Pt{-}CH_3COO + e^- + H^+ \tag{6.12}$$

$$Pt{-}CH_3COO + e^- + H^+ \longrightarrow Pt + CH_3COOH \tag{6.13}$$

7 Conclusion

Electro-oxidation of ethanol was studied by cyclic voltammetry and dynamic electrochemical impedance spectroscopy at different temperatures, with an autoclave set-up.

One observation that could be seen from the results in this work is that the current density for ethanol electro-oxidation increases as the temperature increases. It was also seen an increase in the current density for oxidation as the ethanol concentration increased.

The results of the dynamic electrochemical impedance spectroscopy measurements indicate only one kinetically significant species at the platinum surface in almost all the potential regions where an oxidation current was observed. This, in combination with published literature on ethanol electro-oxidation indicates that the adsorbed intermediate is something other than CO(ads). Published literature on ethanol electro-oxidation reports acetaldehyde and acetic acid as the major products in temperature and concentration ranges looked into during this work. The other adsorbed species at the surface have to be an adsorbed water derivative since the oxidation of ethanol to acetic acid and CO_2 requires one additional oxygen atom.

There was found HNDR behaviour during the negative going scan associated to the presence of a Hopf bifurcation in the electro-oxidation of ethanol at Pt electrodes.

The conclusion that the adsorbed intermediate is something other than CO(ads) and that CO_2 seem to be a small part of the reaction products for ethanol oxidation on platinum indicates that the blocking surface adsorbed species neither is CO(ads). The adsorbed species may rather be another adsorbed ethanol derivative for instance acetate or acetyl. A possible blocking species can be surface adsorbed acetate which has been reported to block the surface by reversible adsorption and de adsorption.

Dynamic electrochemical impedance spectroscopy is a powerful technique for studying reaction mechanisms. It is a mechanism that allows collection of impedance spectra on the fly, which makes it possible to study reactions at partly covered surfaces.

8 Further Work

The following recommendations for further work are given on background of this master thesis work:

An analysis of the EIS data acquired during this work for higher temperatures was not done and an analysis of these data may help elucidate the effect of increasing the temperature on electro-oxidation of ethanol.

It could also be interesting to look into what effects changes in the ethanol concentration will have on the results of dynamic electrochemical impedance spectroscopy measurements, both with higher and lower temperatures. Due to literature suggesting higher CO_2 current efficiency with ethanol concentrations lower than 0.1 M it could be interesting to do dEIS measurements in the same temperature range and with lower concentrations to see if this can give some indications on the mechanism with lower ethanol concentrations. Higher ethanol concentrations may give better resolution of the dEIS data.

Since the experiments done in this work does not give information about the nature of the adsorbed intermediates or the products, only something about the nature of the reactions and the amount of surface adsorbed species it is hard to make a clear conclusion about which products and adsorbed intermediates that is involved in the reactions. A recommendation for further work will therefore be to look more into the nature of the species involved in the reaction. Methods that can tell something about the chemistry of the products and the surface adsorbed species should be done at similar conditions to help give a clearer picture of what the actual surface species in the different potential regions are.

References

[1] C. Lamy, A. Lima, V. LeRhun, F. Delime, C. Coutanceau, and J.-M. Léger. Recent advances in the development of direct alcohol fuel cells (DAFC). *Journal of Power Sources*, 105:283–296, 2002.

[2] C. Lamy, E.M. Belgsir, and J-M. Léger. Electrocatalytic oxidation of aliphatic alcohols: Application to the direct alcohol fuel cell (DAFC). *Journal of Applied Electrochemistry*, 31:799–809, 2001.

[3] U. Krewer, T. Vidakovic-Koch, and L. Rihko-Struckmann. Electrochemical oxidation of Carbon-Containing Fuels and Their Dynamics in Low-Temperature Fuel Cells. *ChemPhysChem*, 12:2518 – 2544, 2011.

[4] F. Vigier, C. Coutanceau, F. Hahn, E. M. Belgsir, and C. Lamy. On the mechanism of ethanol electro-oxidation on Pt and PtSn catalysts: electrochemical and in-situ IR reflectance spectroscopy studies. *Journal of electroanalytical chemistry*, 563:81–89, 2004.

[5] S. C. S. Lai, S. E. F. Kleyn, V. Rosca, and M. T. M. Koper. Mechanism of the Dissociation and Electrooxidation of Ethanol and Acetaldehyde on Platinum As Studied by SERS. *The Journal of Physical Chemistry C*, 112:19080 – 19087, 2008.

[6] H. Wang, Z. Jusys, and J. Behm. Ethanol Electrooxidation on a Carbon-Supported Pt Catalyst: Reaction Kinetics and Product Yields. *The Journal of Physical Chemistry B*, 108:19413 – 19424, 2004.

[7] M. E. Orazem and B. Tribollet. *Electrochemical impedance Spectroscopy*. The Electrochemical Society Series. John Wiley & Sons, 2008.

[8] R. L. Sacci and D. A. Harrington. Dynamic Electrochemical Impedance Spectroscopy. *ECS Transactions*, 19(20):31 – 42, 2009.

[9] J.-M. Léger, C. Coutanceau, and C. Lamy. *Fuel Cell Catalysis: A Surface Science Approach*, chapter 11: Electrocatalysis for the Direct Alcohol Fuel Cell, pages 343 – 373. John Wiley & Sons, Inc., 2011.

[10] C. H. Hamann, A. Hamnett, and W. Vielstich. *Electrochemistry*. WILEY-VCH, 2nd edition, 2007.

[11] P. K. Dahlstrøm. Personal communication, Spring 2012.

[12] A. J. Bard and L. R. Faulkner. *Electrochemical Methods: Fundamentals and Applications*. Wiley, New York, 1980.

[13] A. Lasia. Electrochemical Impedance Spectroscopy and its Applications. In B. E. Conway, J. O'M Bockris, and White R. E., editors, *Modern Aspects of Electrochemistry*, volume 32, pages 143–248. Kluwer Academic/Plenum Publishers, New York, 1999.

[14] D. A. Harrington. Electrochemical impedance spectroscopy. Lecture notes from a course about electrochemical impedance spectroscopy at NTNU.

[15] Harrington, D. A. Ac voltammetry for measurement of surface kinetics. *Journal of Electroanalytical Chemistry*, 355(1 - 2):21 – 35, 1993.

[16] D. Roy, J. E. Garland, and C. M. Pettit. Analysis of experimental constraints and variables for time resolved detection of Fourier transform electrochemical impedance spectra. *Electrochimica Acta*, 49:2623 – 2635, 2004.

[17] H-J. Butt, K. Graf, and M. Kappl. *Physics and Chemistry of Interfaces*. WILEY-VCH, 1st edition, 2006.

[18] X.-Z. Yuan, C. Song, H. Wang, and J. Zhang. *Electrochemical Impedance Spectroscopy in PEM Fuel Cells*, chapter 4. Springer London, 2010.

[19] R. E. Melnick and G. T. R. Palmore. Impedance spectroscopy of the electro-oxidation of methanol on polished polycrystalline platinum. *The Journal of Physical Chemistry B*, 105(5):1012–1025, 2001.

[20] H. Hitmi, E. M. Belgsir, J.-M. Léger, C. Lamy, and R. O. Lezna. A kinetic analysis of the electro-oxidation of ethanol at a platinum electrode in acid medium. *Electrochimica Acta*, 39(3):407 – 415, 1994.

[21] R. Brateng. Electrooxidation of methanol and ethanol. Technical report, Norwegian University of Science and Technology, 2004-2005.

[22] G. A. Camara and T. Iwasita. Parallel pathways of ethanol oxidation: The effect of ethanol concentration. *Journal of Electroanalytical Chemistry*, 578: 315 – 321, 2005.

[23] F. Colmati, E. Antolini, and E. R. Gonzalez. Effect of temperature on the mechanism of ethanol oxidation on carbon supported Pt, PtRu and Pt_3Sn electrocatalysts. *Journal of Power Sources*, 157:98 – 103, 2006.

[24] S. Sun, M. C. Halseid, M. Heinen, Z. Jusys, and R. J. Behm. Ethanol electrooxidation on e carbon-supported Pt catalyst at elevated temperatures and pressure: A high-temperature/high-pressure DEMS study. *Journal of Power Sources*, 190:2 – 13, 2009.

[25] B. Pierozynski. Kinetic Aspects of Ethanol Electrooxidation on Catalytic Surfaces of Pt in 0.5 M H_2SO_4. *International Journal of Electrochemical Science*, 7:3327 – 3338, 2012.

[26] F. Seland, R. Tunold, and D. A. Harrington. Impedance study of methanol oxidation on platinum electrodes. *Electrochimica Acta*, 51:3827 – 3840, 2006.

[27] P. R. Bevington. *Data Reduction and Error Analysis for the Physical Sciences*. McGraw-Hill Book Company, 1969.

[28] F. Seland. Personal communication, Spring 2012.

[29] F. Seland, R. Tunold, and D. A. Harrington. Impedance study of formic acid oxidation on platinum electrodes. *Electrochimica Acta*, 53:6851 – 6864, 2006.

[30] R. J. Behm and Z. Jusys. The potential of model studies for the understanding of catalyst poisoning and temperature effects in polymer electrolyte fuel cell reactions. *Journal of Power Sources*, 2006.

[31] D. Bokach, J. L. G. de la Fuente, M. Tsypkin, P. Ochal, I. C. Endsjø, R. Tunold, S. Sunde, and F. Seland. High-Temperature Electrochemical Characterization of Ru Core Pt Shell Fuel Cell Catalyst. *Fuel Cells*, 11: 735–744, 2011.

[32] M. Alsabet, M. Grden, and G. Jerkiewicz. Comprehensive study of the growth of thin oxide layers on pt electrodes under well-defined temperature, potential, and time conditions. *Journal of Electroanalytical Chemistry*, 589:120 – 127, 2006.

[33] J. L. Cohen, D. J. Volpe, and H. D. Abruña. Electrochemical determination of activation energies for methanol oxidation on polycrystalline platinum in acidic and alkaline electrolytes. *Physical Chemistry Chemical Physics*, 9:49 – 77, 2007.

[34] F. Seland. Oxidation of Small Organic Molecules by Dynamic Electrochemical Impedance Spectroscopy, 2012. Presentation held at the 221st ECS Meeting, Seattle.

[35] B. E. Conway and G. Jerkiewicz. Surface orientation dependence of oxide film growth at platinum single crystals. *Journal of Electroanalytical Chemistry*, 339 (1–2):123 – 146, 1992.

[36] K. Krischer and H. Varela. *Electrocatalysis*, volume 2 of *Handbook of Fuel Cells – Fundamentals and Applications*, chapter 46: Oscillations and other dynamic instabilities. John Wiley and Sons, 2003.

[37] M. T. M. Koper. Oscillations and complex dynamical bifurcations in electrochemical systems. *Advances in Chemical Physics*, 92:161, 1996.

[38] M. Heinen, Z. Jusys, and R. J. Behm. Ethanol, Acetaldehyde and Acetic Acid Adsorption/Electrooxidation on a Pt Thin Film Electrode under Continuous Electrolyte Flow: An in Situ ATR-FTIRS Flow Cell Study. *Journal of Physical Chemistry C*, 114:9850 – 9864, 2010.

A Calculation of Surface Area

The experimental calculation of the real active surface area of the working electrode was made with the assumption that one hydrogen atom adsorbs at each surface platinum atom [10]. The estimation of the surface area was done by calculating the charge for the hydrogen adsorption peaks. This was assessed from a cyclic voltammogram at 100 mV/s by use of Echem analyst as shown in Figure A.1. As a correction of the double layer charging it was made a horizontal line with the linear fit function that is built in in Echem analyst. The charge was then calculated by use of the built in integration function. To calculate the surface area the charge was then divided by the hydrogen capacity which is taken to be 220 $\mu C/cm^2$ for platinum [11]. The calculation of the surface area was done for each temperature before addition of ethanol.

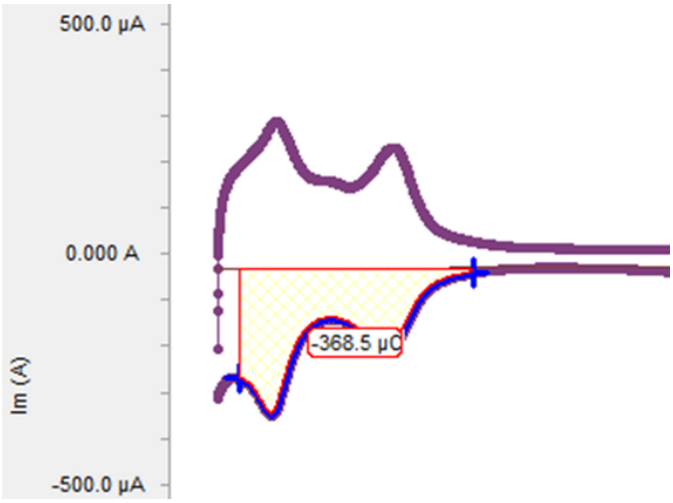

Figure A.1: The section of a voltammogram of Pt in 0.5 M sulphuric acid at 100 mV/s used for the integration of charge for calculation of the active surface area

B Additional Dynamic Electrochemical Impedance Spectroscopy (dEIS) Measurements

In addition to dynamic electrochemical impedance spectroscopy (dEIS) with sweep rate of 1 mV/s at 60°C dEIS was also done with a sweep rate of 5 and 10 mV/s.

Figure B.1 (a) gives a summary of the electrochemical impedance behaviour correlated to the cyclic voltammogram of 0.2 M ethanol at 60°C with 5 mV/s sweep rate. And Figure B.1 (b) gives a summary of the impedance behaviour for the same concentration and temperature with sweep rate of 10 mV/s.

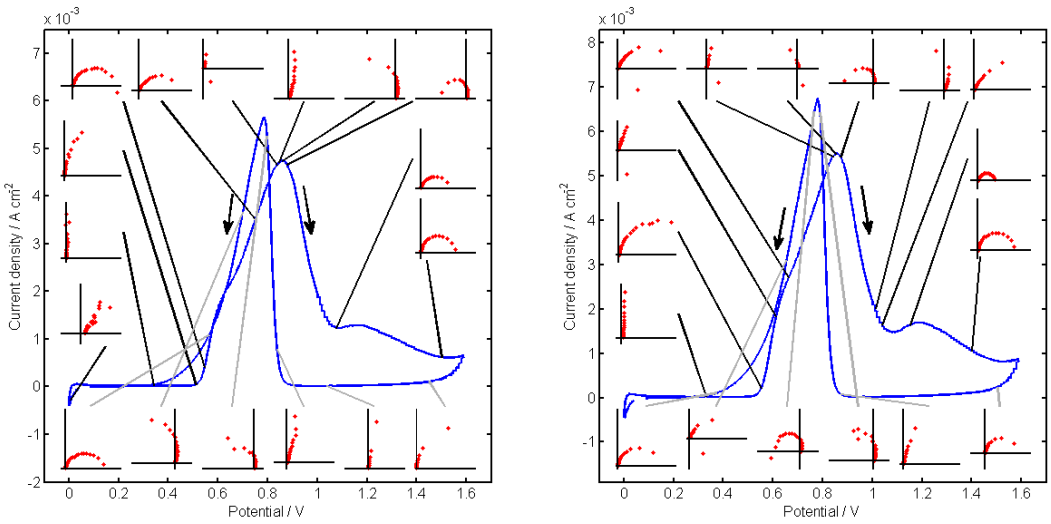

(a) (b)

Figure B.1: Summary of impedance behaviour for 0.2 M ethanol with respect to the cyclic voltammogram at 60°C with sweep rate of (a) 5 mV/s (b) 10 mV/s